arXiv:1409.1697v1 [hep-ph] 5 Sep 2014

STUPP-14-218
September 8, 2014

A way to crosscheck μ-e conversion in the case of no signals of $\mu \to e\gamma$ and $\mu \to 3e$

Joe Sato[a, 1], and **Masato Yamanaka**[b, 2]

[a] *Department of Physics, Saitama University, Shimo-okubo, Sakura-ku, Saitama, 338-8570, Japan*

[b] *Department of Physics, Nagoya University, Nagoya 464-8602, Japan*

Abstract

We consider the case that μ-e conversion signal is discovered but other charged lepton flavor violating (cLFV) processes will never be found. In such a case, we need other approaches to confirm the μ-e conversion and its underlying physics without conventional cLFV searches. We study R-parity violating (RPV) SUSY models as a benchmark. We briefly review that our interesting case is realized in RPV SUSY models with reasonable settings according to current theoretical/experimental status. We focus on the exotic collider signatures at the LHC ($pp \to \mu^- e^+$ and $pp \to jj$) as the other approaches. We show the correlations between the branching ratio of μ-e conversion process and cross sections of these processes. It is first time that the correlations are graphically shown. We exhibit the RPV parameter dependence of the branching ratio and the cross sections, and discuss the feasibility to determine the parameters.

[1] joe@phy.saitama-u.ac.jp
[2] yamanaka@eken.phys.nagoya-u.ac.jp

Contents

1 Introduction **1**

2 RPV interaction and our scenario **2**

3 Exotic processes in our scenario **3**
3.1 μ-e conversion 4
3.2 $pp \to \mu^- e^+$ and $pp \to jj$ 6
3.3 NSI 9
3.4 Muonium conversion 10

4 Numerical result **10**
4.1 Case-I ($\lambda'_{311} \neq 0$, $\lambda'_{322} = 0$) 11
4.2 Case-II ($\lambda'_{311} = 0$ and $\lambda'_{322} \neq 0$) 15
4.3 Case-III ($\lambda'_{311} \neq 0$ and $\lambda'_{322} \neq 0$) 18
4.4 comment for NSI 18

5 Summary and discussion **22**

1 Introduction

Lepton flavor violation (LFV) is the clearest signal for physics beyond the Standard Model (SM) as it conserves lepton flavor exactly [1]. Therefore extensive searches for LFV have been made since the muon was found. There have been searches for $\mu \to e\gamma$ [2, 3] , $\mu - e$ conversion [4] and $\mu \to 3e$ [5] . In all of these processes both muon and electron number are violated. There are also LFV searches with the tau lepton [6, 7, 8, 9] . Though a lot of efforts have been made, we have not found any LFV signals with charged leptons. LFV had, however, been found in neutrino oscillation [10, 11] and it indeed requires us to extend the SM so that physics beyond the SM must include LFV. This fact also gives us a strong motivation to search for charged lepton flavor violation (cLFV). Indeed the MEG collaboration has tried to observe the process $\mu \to e\gamma$ and gave a significant upper bound on its branching ratio [3] . Another effort at the LHC gave some of upper limits on tau number violation [12] though at this moment more stringent limits are given by Belle collaboration.

Along this line new experiments to search for cLFV will start soon. COMET [13, 14] and DeeMe [15] will launch within a few years and search $\mu - e$ conversion. In these experiments, first, muons are trapped by target nucleus (carbon, aluminum, titanium, and so on), then, if cLFV exists, it converts into an electron.

If COMET and DeeMe observe the conversion process, then with what kind of new physics should we interpret it? Now it is worth considering again since we are in-between two kinds of cLFV experiments with muon.

For these several decades, theories with supersymmetric extension have been most studied. These theories include a source of LFV. It is realized by the fact that the scalar partner of the charged leptons can have a different flavor basis from that of the charged leptons. In addition, R-parity is often imposed on this class of the theory[16, 17]. With it, $\mu \to e\gamma$ process has the largest branching ratio among the three cLFV processes. This occurs through the dipole process

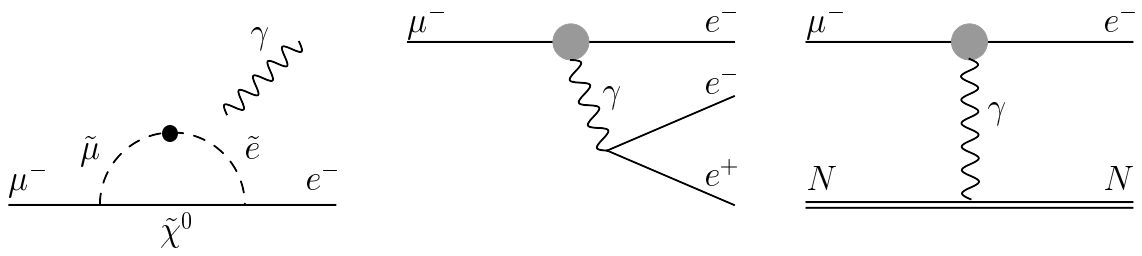

Figure 1: cLFV processes in supersymmetric models with R-parity conservation.

depicted in Fig. 1 and the other two, $\mu-e$ conversion and $\mu \to 3e$ are realized by attaching a quark line and an electron line at the end of the photon line respectively, giving an $\mathrm{O}(\alpha)$ suppression. Those branching ratios must be smaller than that of $\mu \to e\gamma$. At this moment, however, the upper bounds for those branching ratios are almost same each other. It means if COMET and DeeMe observe a cLFV, that is the $\mu - e$ conversion process, we have to discard this scenario.

It is, however, possible to find a theory easily in which COMET/DeeMe find cLFV first. To see this we first note that the $\mu \to e\gamma$ process occurs only at loop level due to the gauge invariance, while other two can occur as a tree process. Therefore in this case we have to consider a theory in which the $\mu - e$ conversion process occurs as tree process. In other words we have to assume a particle which violate muon and electron number. Since $\mu - e$ conversion occurs in a nucleus, it also couples with quarks with flavor conservation. Furthermore it is better to assume that it does not couple with two electrons as we have not observed $\mu \to 3e$.

In this paper we consider the case that COMET/DeeMe indeed observe the cLFV process, while all the other experiments will not observe anything new at that time. With this situation, we need to understand how to confirm the cLFV in other experiments. It is dependent on a theory considered. Unfortunately in this case other new physics signals are expected to be quite few, since the magnitude of the cLFV interaction is so small due to its tiny branching ratio. Therefore it is very important to simulate now how to confirm the COMET signal and the new physics. As a benchmark case we study a supersymmetric standard model without R parity [18] . In this kind of theory the scalar lepton mediates $\mu \leftrightarrow e$ flavor violation. It is important to emphasize that the R parity violating theory is strongly motivated by also the fact that we have not observed any typical SUSY signals.

The paper is organized as follows. First, in Sec. 2 we briefly review a theory with R parity violation and show our setup. Next, in Sec. 3 we discuss what processes can be the signal of the theory. Then in Sec. 4 we give the result and discuss how to confirm the scenario here depending on the parameters. Finally we summarize our work in Sec. 5.

2 RPV interaction and our scenario

In general the supersymmetric gauge invariant superpotential contains the R-parity violating terms [19, 20, 21],

$$\mathcal{W}_{\mathrm{RPV}} = \lambda_{ijk} L_i L_j E^c_k + \lambda'_{ijk} L_i Q_j D^c_k + \lambda''_{ijk} U^c_i D^c_j D^c_k, \tag{1}$$

where E^c_i, U^c_i and D^c_i are $SU(2)_L$ singlet superfields, and L_i and Q_i are $SU(2)_L$ doublet superfields. Indices i, j, and k represent the generations. We take $\lambda_{ijk} = -\lambda_{jik}$ and $\lambda''_{ijk} = -\lambda''_{ikj}$. First

two terms include lepton number violation, and the last term includes baryon number violation. Since some combinations of them accelerate proton decay, we omit the last term. Thus the RPV processes are described by following Lagrangian,

$$\begin{aligned}
&\mathcal{L}_{\rm RPV} = \mathcal{L}_\lambda + \mathcal{L}_{\lambda'},\\
&\mathcal{L}_\lambda = \lambda_{ijk}\big[\tilde{\nu}_{iL}\overline{e}_{kR}e_{jL} + \tilde{e}_{jL}\overline{e}_{kR}\nu_{iL} + \tilde{e}^*_{kR}\overline{(\nu_{iL})^c}e_{jL} - (i \leftrightarrow j)\big] + \text{h.c.},\\
&\mathcal{L}_{\lambda'} = \lambda'_{ijk}\big[\tilde{\nu}_{iL}\overline{d}_{kR}d_{jL} + \tilde{d}_{jL}\overline{d}_{kR}\nu_{iL} + \tilde{d}^*_{kR}\overline{(\nu_{iL})^c}d_{jL}\\
&\qquad - \tilde{e}_{iL}\overline{d}_{kR}u_{jL} - \tilde{u}_{jL}\overline{d}_{kR}e_{jL} - \tilde{d}^*_{kR}\overline{(e_{iL})^c}u_{jL}\big] + \text{h.c.}.
\end{aligned} \tag{2}$$

Our interesting situation is that only μ-e conversion is discovered, and other cLFV processes will never be observed. The situation is realized under the following 3 setting on the RPV interaction:

1. only the third generation slepton contributes to the RPV interactions
2. for quarks, flavor diagonal components are much larger than that of off-diagonal components, i.e., CKM-like matrix, $\lambda'_{ijj} \gg \lambda'_{ijk}(j \neq k)$
3. the generation between left-handed and right-handed leptons are different, $\lambda_{ijk}(i \neq k \text{ and } j \neq k)$.

The setting-1 is naturally realized by the RG evolved SUSY spectrum with universal soft masses at the GUT scale. For the simplicity, we decouple other SUSY particles except for the third generation sleptons. The setting-2 is also obtained in most cases unless we introduce additional sources of flavor violations. The setting-3 is artificially introduced to realize the interesting situation in this work, that the COMET find the cLFV process, while all the other experiments will not observe anything new at that time (see Introduction). Under the settings, the general Lagrangian (2) is reduced as follows,

$$\begin{aligned}
&\mathcal{L}_{\rm RPV} = \mathcal{L}_\lambda + \mathcal{L}_{\lambda'},\\
&\mathcal{L}_\lambda = 2\big[\lambda_{312}\tilde{\nu}_{\tau L}\overline{\mu}P_L e + \lambda_{321}\tilde{\nu}_{\tau L}\overline{e}P_L\mu + \lambda_{132}\tilde{\tau}_L\overline{\mu}P_L\nu_e + \lambda_{231}\tilde{\tau}_L\overline{e}P_L\nu_\mu\\
&\qquad + \lambda_{123}\tilde{\tau}^*_R\overline{(\nu_{eL})^c}P_L\mu + \lambda_{213}\tilde{\tau}^*_R\overline{(\nu_{\mu L})^c}P_L e\big] + \text{h.c.},\\
&\mathcal{L}_{\lambda'} = \big[\lambda'_{311}\big(\tilde{\nu}_{\tau L}\overline{d}P_L d - \tilde{\tau}_L\overline{d}P_L u\big) + \lambda'_{322}\big(\tilde{\nu}_{\tau L}\overline{s}P_L s - \tilde{\tau}_L\overline{s}P_L c\big)\big] + \text{h.c.}.
\end{aligned} \tag{3}$$

Some kind of processes described by the Lagrangian (3) strongly depend on the values of λ'_{311} and λ'_{322}. In this work, to clarify the dependence and to discuss the discrimination of each other, we study three cases:

case-I	$\lambda'_{311} \neq 0$ and $\lambda'_{322} = 0$
case-II	$\lambda'_{311} = 0$ and $\lambda'_{322} \neq 0$
case-III	$\lambda'_{311} \neq 0$ and $\lambda'_{322} \neq 0$

3 Exotic processes in our scenario

In our scenario we may have five types of exotic processes: μ-e conversion in a nucleus, $pp \to \mu^- e^+$, $pp \to jj$, non-standard interaction (NSI) of neutrinos, and muonium conversion $\mu^+e^- \leftrightarrow \mu^- e^+$. We formulate each reaction rate in our scenario.

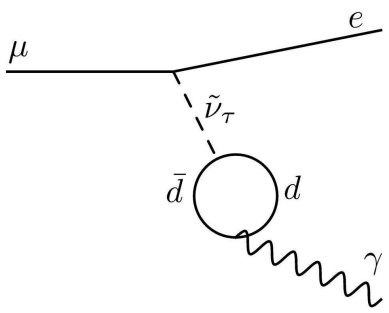

Figure 2: Possible one-loop diagram for $\mu \to e\gamma$. It is , however, proportional to $q^2 q^\mu$ and hence vanish with on-shell photon ($q^2 = 0$) and with $\bar{e}\gamma_\mu e$ attached due to gauge symmetry.

Note that in our scenario other muon cLFV processes ($\mu \to e\gamma$, $\mu \to 3e$, $\mu^- e^- \to e^- e^-$ in muonic atom [22], and so on) occur at two-loop level. At one glance the tau sneutrino can connect with the photon via d-quark loop shown in Fig. 2. The contribution of the loop of the diagram is

$$\lambda' \left(-\frac{1}{3}\right) e \frac{m_d q_\mu}{8\pi^2} \int_0^1 dx (1-2x) \log(m_d^2 - (x - x^2)q^2) \ \propto q^2 q^\mu, \tag{4}$$

where q is the four-momentum of the photon. The contribution to cLFV is, therefore vanish with on-shell photon ($q^2 = 0$) for $\mu \to e\gamma$ and with $\bar{e}\gamma_\mu e$ attached for $\mu \to 3e$ due to gauge symmetry($q^\mu \bar{e}\gamma_\mu e = 0$).

Thus these processes occur at two-loop level. Furthermore these loop processes are extremely suppressed further by higher order couplings, gauge invariance, and so on. Therefore we do not study these processes here.

3.1 μ-e conversion

We briefly review the formulation of the branching ratio of μ-e conversion process based on Refs. [23, 24]. The μ-e conversion process via the tau sneutrino exchange is described by the effective interaction Lagrangian

$$\mathcal{L}_{int} = -\frac{G_F}{\sqrt{2}} \sum_{q=d,s} \left\{ \left(g_{LS(q)} \bar{e} P_R \mu + g_{RS(q)} \bar{e} P_L \mu \right) \bar{q} q \right\} + \text{h.c.}, \tag{5}$$

where G_F is the Fermi coupling constant. The coefficients $g_{LS(q)}$ and $g_{RS(q)}$ are derived from the RPV interaction Lagrangian [Eq. (3)],

$$g_{LS(d)} = \frac{\sqrt{2}}{G_F} \frac{2}{m^2_{\tilde{\nu}_\tau}} \lambda'_{311} \lambda^*_{312}, \tag{6}$$

$$g_{RS(d)} = \frac{\sqrt{2}}{G_F} \frac{2}{m^2_{\tilde{\nu}_\tau}} \lambda'^*_{311} \lambda_{321}, \tag{7}$$

$$g_{LS(s)} = \frac{\sqrt{2}}{G_F} \frac{2}{m^2_{\tilde{\nu}_\tau}} \lambda'_{322} \lambda^*_{312}, \tag{8}$$

$$g_{RS(s)} = \frac{\sqrt{2}}{G_F} \frac{2}{m^2_{\tilde{\nu}_\tau}} \lambda'^*_{322} \lambda_{321}. \tag{9}$$

The amplitude for the μ-e conversion process is calculated by the overlap of wave functions of the initial state muon $\psi_{1S}^{(\mu)}$, the final state electron $\psi_{\kappa,W}^{\mu(e)}$ with the eigenvalues of the orbital angular momentum $-\kappa$ and of the z-component angular momentum μ, and the initial and final state nucleus as follows

$$\mathcal{M} = \frac{G_F}{\sqrt{2}} \sum_{q=d,s} \int d^3\boldsymbol{x} \left(g_{LS(q)} \bar{\psi}_{\kappa,W}^{\mu(e)} P_R \psi_{1S}^{(\mu)} + g_{RS(q)} \bar{\psi}_{\kappa,W}^{\mu(e)} P_L \psi_{1S}^{(\mu)} \right) \langle N|\bar{q}q|N\rangle. \tag{10}$$

Here we omitted the incoherent conversion process, because its fraction is much smaller than the coherent one. The matrix element $\langle N|\bar{q}q|N\rangle$ is given by the atomic number Z, the mass number A, and the proton (neutron) density in nucleus $\rho^{(p)}$ ($\rho^{(n)}$),

$$\langle N|\bar{q}q|N\rangle = Z G_S^{(q,p)} \rho^{(p)} + (A-Z) G_S^{(q,n)} \rho^{(n)}. \tag{11}$$

The coefficients for scalar operators are evaluated in Ref. [25]: $G_S^{(d,n)} = 5.1$, $G_S^{(d,p)} = 4.3$, and $G_S^{(s,p)} = G_S^{(s,n)} = 2.5$. This calculation assumes that the proton and the neutron densities are in spherical distribution and normalized as $\int dr 4\pi r^2 \rho^{(p,n)} = 1$.

The reaction rate of the μ-e conversion is

$$\omega_{conv} = 2G_F^2 \left| \tilde{g}_{LS}^{(p)} S^{(p)} + \tilde{g}_{LS}^{(n)} S^{(n)} \right|^2 + 2G_F^2 \left| \tilde{g}_{RS}^{(p)} S^{(p)} + \tilde{g}_{RS}^{(n)} S^{(n)} \right|^2. \tag{12}$$

The overlap integral of wave functions of muon, electron, and protons (neutrons) gives $S^{(p)}$ ($S^{(n)}$) (explicit formulae and details of the calculation are explained in Ref. [24]). We list $S^{(p)}$ and $S^{(n)}$ for relevant nuclei of SINDRUM-Ⅱ (Au), DeeMe (C and Si), COMET (Al and Ti), Mu2e (Al and Ti), and PRISM (Al and Ti) in Table 1. The coefficients $\tilde{g}_{LS,RS}^{(p)}$ and $\tilde{g}_{LS,RS}^{(n)}$ are

$$\tilde{g}_{LS,RS}^{(p)} = \sum_q G_S^{q,p} g_{LS,RS(q)} = G_S^{d,p} g_{LS,RS(d)} + G_S^{s,p} g_{LS,RS(s)}, \tag{13}$$

$$\tilde{g}_{LS,RS}^{(n)} = \sum_q G_S^{q,n} g_{LS,RS(q)} = G_S^{d,n} g_{LS,RS(d)} + G_S^{s,n} g_{LS,RS(s)}. \tag{14}$$

Thus the reaction rate of μ-e conversion via the $\tilde{\nu}_\tau$ exchange is obtained as follows,

$$\begin{aligned} \omega_{conv} = &\frac{16}{m_{\tilde{\nu}_\tau}^4} \left| (4.3S^{(p)} + 5.1S^{(n)}) \lambda'_{311} \lambda^*_{312} + 2.5(S^{(p)} + S^{(n)}) \lambda'_{322} \lambda^*_{312} \right|^2 \\ &+ \frac{16}{m_{\tilde{\nu}_\tau}^4} \left| (4.3S^{(p)} + 5.1S^{(n)}) \lambda'^*_{311} \lambda_{321} + 2.5(S^{(p)} + S^{(n)}) \lambda'^*_{322} \lambda_{321} \right|^2. \end{aligned} \tag{15}$$

The branching ratio of μ-e conversion process is defined by

$$\mathrm{BR}(\mu^- N \to e^- N) = \omega_{conv} / \omega_{capt}, \tag{16}$$

where ω_{capt} is the muon capture rate of nucleus. We list the values of ω_{capt} in Table 1. Assuming λ'_{311} and λ'_{322} are real and $\lambda^*_{312} = \lambda_{321} \equiv \lambda$, the branching ratio for $N = \mathrm{C}$ is given by

$$\begin{aligned} \mathrm{BR}(\mu^- \mathrm{C} \to e^- \mathrm{C}) &= 1.383 \times 10^{-15} \left(\frac{1\mathrm{TeV}}{m_{\tilde{\nu}_\tau}} \right)^4 \left(\frac{\lambda'_{311} \lambda}{10^{-8}} \right)^2 \left| 1 + 0.532 \left(\frac{\lambda'_{322}}{\lambda'_{311}} \right) \right|^2 \\ &= 3.913 \times 10^{-16} \left(\frac{1\mathrm{TeV}}{m_{\tilde{\nu}_\tau}} \right)^4 \left(\frac{\lambda'_{322} \lambda}{10^{-8}} \right)^2 \left| 1 + 1.880 \left(\frac{\lambda'_{311}}{\lambda'_{322}} \right) \right|^2, \end{aligned} \tag{17}$$

for $N = \mathrm{Al}$,

$$\begin{aligned}\mathrm{BR}(\mu^- \mathrm{Al} \to e^- \mathrm{Al}) &= 2.092 \times 10^{-15} \left(\frac{1\mathrm{TeV}}{m_{\tilde{\nu}_\tau}}\right)^4 \left(\frac{\lambda'_{311}\lambda}{10^{-8}}\right)^2 \left|1 + 0.530 \left(\frac{\lambda'_{322}}{\lambda'_{311}}\right)\right|^2 \\ &= 5.881 \times 10^{-16} \left(\frac{1\mathrm{TeV}}{m_{\tilde{\nu}_\tau}}\right)^4 \left(\frac{\lambda'_{322}\lambda}{10^{-8}}\right)^2 \left|1 + 1.886 \left(\frac{\lambda'_{311}}{\lambda'_{322}}\right)\right|^2,\end{aligned} \tag{18}$$

for $N = \mathrm{Si}$,

$$\begin{aligned}\mathrm{BR}(\mu^- \mathrm{Si} \to e^- \mathrm{Si}) &= 2.080 \times 10^{-15} \left(\frac{1\mathrm{TeV}}{m_{\tilde{\nu}_\tau}}\right)^4 \left(\frac{\lambda'_{311}\lambda}{10^{-8}}\right)^2 \left|1 + 0.532 \left(\frac{\lambda'_{322}}{\lambda'_{311}}\right)\right|^2 \\ &= 5.886 \times 10^{-16} \left(\frac{1\mathrm{TeV}}{m_{\tilde{\nu}_\tau}}\right)^4 \left(\frac{\lambda'_{322}\lambda}{10^{-8}}\right)^2 \left|1 + 1.880 \left(\frac{\lambda'_{311}}{\lambda'_{322}}\right)\right|^2,\end{aligned} \tag{19}$$

and for $N = \mathrm{Ti}$,

$$\begin{aligned}\mathrm{BR}(\mu^- \mathrm{Ti} \to e^- \mathrm{Ti}) &= 3.571 \times 10^{-15} \left(\frac{1\mathrm{TeV}}{m_{\tilde{\nu}_\tau}}\right)^4 \left(\frac{\lambda'_{311}\lambda}{10^{-8}}\right)^2 \left|1 + 0.528 \left(\frac{\lambda'_{322}}{\lambda'_{311}}\right)\right|^2 \\ &= 9.962 \times 10^{-16} \left(\frac{1\mathrm{TeV}}{m_{\tilde{\nu}_\tau}}\right)^4 \left(\frac{\lambda'_{322}\lambda}{10^{-8}}\right)^2 \left|1 + 1.893 \left(\frac{\lambda'_{311}}{\lambda'_{322}}\right)\right|^2.\end{aligned} \tag{20}$$

Table 1: The overlap factor of wave functions (explicit formulae and details of the calculation are explained in Ref. [24]) and the muon capture rate ω_{capt} for each nucleus. Here m_μ is muon mass.

Nucleus	$S^{(p)}$	$S^{(n)}$	$\omega_{capt}(s^{-1})$
C	$0.00308 m_\mu^{5/2}$	$0.00308 m_\mu^{5/2}$	0.388×10^5
Si	$0.0179 m_\mu^{5/2}$	$0.0179 m_\mu^{5/2}$	8.712×10^5
Al	$0.0155 m_\mu^{5/2}$	$0.0167 m_\mu^{5/2}$	7.054×10^5
Ti	$0.0368 m_\mu^{5/2}$	$0.0435 m_\mu^{5/2}$	2.590×10^6
Au	$0.0614 m_\mu^{5/2}$	$0.0918 m_\mu^{5/2}$	1.307×10^7

3.2 $pp \to \mu^- e^+$ and $pp \to jj$

We formulate the cross sections of $pp \to \mu^- e^+$ and $pp \to jj$ in the RPV scenario. In the scenario, these processes are dominated by s-channel exchange resonance, and hence the cross sections are well approximated by the Breit-Wigner formula. The cross section for a final state $f_1 f_2$ is decomposed with $\gamma_{\tilde{\nu}_\tau} = \Gamma_{\tilde{\nu}_\tau}/m_{\tilde{\nu}_\tau}$ as follows

$$\begin{aligned}\sigma(pp \to f_1 f_2) &= F(\sqrt{s}, m_{\tilde{\nu}_\tau}, q_1, q_2) \times \Gamma_{\tilde{\nu}_\tau} \mathrm{BR}(\tilde{\nu}_\tau \to q_1 q_2) \mathrm{BR}(\tilde{\nu}_\tau \to f_1 f_2) \\ &= F(\sqrt{s}, m_{\tilde{\nu}_\tau}, q_1, q_2) m_{\tilde{\nu}_\tau} \times \gamma_{\tilde{\nu}_\tau} \mathrm{BR}(\tilde{\nu}_\tau \to q_1 q_2) \mathrm{BR}(\tilde{\nu}_\tau \to f_1 f_2)\end{aligned} \tag{21}$$

The front part, $F(\sqrt{s}, m_{\tilde{\nu}_\tau}, q_1, q_2) m_{\tilde{\nu}_\tau}$, is determined by the kinematics of each process, and is a function of collision energy $\sqrt{s}$, mediator mass $m_{\tilde{\nu}_\tau}$, and the flavors of initial quarks (q_1 and q_2). The decay width $\Gamma_{\tilde{\nu}_{\tau L}}$ is calculated by the Lagrangian [Eq. (3)],

$$\Gamma_{\tilde{\nu}_{\tau L}} = \frac{m_{\tilde{\nu}_{\tau L}}}{16\pi} \left(3\lambda'^2_{311} + 3\lambda'^2_{322} + 4\lambda^2_{312} + 4\lambda^2_{321}\right). \tag{22}$$

The remaining part, $\gamma_{\tilde{\nu}_\tau}\mathrm{BR}(\tilde{\nu}_\tau \to q_1 q_2)\mathrm{BR}(\tilde{\nu}_\tau \to f_1 f_2)$, depends only on the coupling constants of RPV interactions.

First we formulate $F(\sqrt{s}, m_{\tilde{\nu}_\tau}, q_1, q_2)$. With regardless of final state, once $\sqrt{s}$, $m_{\tilde{\nu}_\tau}$, and an initial state are fixed, $F(\sqrt{s}, m_{\tilde{\nu}_\tau}, q_1, q_2)$ is uniquely determined. It is really important and useful for analyzing the RPV coupling dependence on the cross sections to derive the explicit formula of $F(\sqrt{s}, m_{\tilde{\nu}_\tau}, q_1, q_2)$. The expression of $F(\sqrt{s}, m_{\tilde{\nu}_\tau}, q_1, q_2)$ is given from Eq. (21),

$$F(\sqrt{s}, m_{\tilde{\nu}_\tau}, q_1, q_2) = \frac{\sigma(pp \to f_1 f_2)}{m_{\tilde{\nu}_\tau}\gamma_{\tilde{\nu}_\tau}\mathrm{BR}(\tilde{\nu}_\tau \to q_1 q_2)\mathrm{BR}(\tilde{\nu}_\tau \to f_1 f_2)}. \tag{23}$$

Numerical results from Eq. (23) are shown by rotated squares in Fig. 3. In Fig. 3, we use an abbreviation $F_{q_1 q_2}$ as $F(\sqrt{s}, m_{\tilde{\nu}_\tau}, q_1, q_2)$. For each set of $\sqrt{s}$ and initial state quarks, we can parameterize $F(\sqrt{s}, m_{\tilde{\nu}_\tau}, q_1, q_2)$ as a function of $m_{\tilde{\nu}_\tau}$ as follows,

$$F(\sqrt{s}, m_{\tilde{\nu}_\tau}, q_1, q_2) = \alpha \times 10^{-\beta m_{\tilde{\nu}_\tau}} m_{\tilde{\nu}_\tau}^{-\gamma}\ [\mathrm{pb}\cdot\mathrm{GeV}^{-1}]\,, \tag{24}$$

where coefficients α, β, and γ are calculated from numerical calculations of $F(\sqrt{s}, m_{\tilde{\nu}_\tau}, q_1, q_2)$, and we list the coefficients in table 2. The fitted function of $F(\sqrt{s}, m_{\tilde{\nu}_\tau}, q_1, q_2)$ for collision energy $\sqrt{s} = 14\mathrm{TeV}$ and $\sqrt{s} = 100\mathrm{TeV}$ are shown by lines in Fig. 3.

Table 2: The coefficients for fit function of $F(\sqrt{s}, m_{\tilde{\nu}_\tau}, q_1, q_2)$ (see Eq. (23)) for each set of the collision energy $\sqrt{s}$ and initial state quarks. We use CTEQ6L parton distribution function [26] for the evaluation.

$(\sqrt{s},\ q_1,\ q_2)$	$\alpha\ [\mathrm{pb}\cdot\mathrm{GeV}^{\gamma-1}]$	$\beta\ [\mathrm{GeV}^{-1}]$	γ
$(14\mathrm{TeV}, d, \bar{d})$	1.352×10^{11}	6.500×10^{-4}	3.480
$(14\mathrm{TeV}, u, \bar{d})$	6.652×10^{10}	5.900×10^{-4}	3.400
$(14\mathrm{TeV}, d, \bar{u})$	2.233×10^{11}	5.800×10^{-4}	3.700
$(14\mathrm{TeV}, s, \bar{s})$	2.248×10^{12}	7.600×10^{-4}	4.200
$(100\mathrm{TeV}, d, \bar{d})$	2.220×10^{13}	8.000×10^{-5}	4.000
$(100\mathrm{TeV}, u, \bar{d})$	8.385×10^{12}	7.500×10^{-5}	3.900
$(100\mathrm{TeV}, d, \bar{u})$	1.084×10^{13}	8.500×10^{-5}	4.000
$(100\mathrm{TeV}, s, \bar{s})$	3.265×10^{13}	1.400×10^{-4}	4.200

From Eq. (21), the cross section of $pp \to \mu^- e^+$ is analytically calculated with the decay rate [Eq. (22)] and the fit function of $F(\sqrt{s}, m_{\tilde{\nu}_\tau}, q_1, q_2)$ [Eq. (24)] as follows,

$$\begin{aligned}\sigma(pp \to \mu^- e^+) = \sum_{i=1,2} \Big\{ & F(\sqrt{s}, m_{\tilde{\nu}_\tau}, d_i, \bar{d}_i) m_{\tilde{\nu}_\tau} \times \frac{1}{16\pi}\left(3\lambda'^2_{311} + 3\lambda'^2_{322} + 4\lambda^2_{312} + 4\lambda^2_{321}\right) \\ & \times \frac{3\lambda'^2_{3ii}}{3\lambda'^2_{311} + 3\lambda'^2_{322} + 4\lambda^2_{312} + 4\lambda^2_{321}} \cdot \frac{4\lambda^2_{312}}{3\lambda'^2_{311} + 3\lambda'^2_{322} + 4\lambda^2_{312} + 4\lambda^2_{321}} \Big\}.\end{aligned} \tag{25}$$

Here $d_1 = d$ and $d_2 = s$. The cross section of dijet production, $\sigma(pp \to jj)$, is similarly calculated

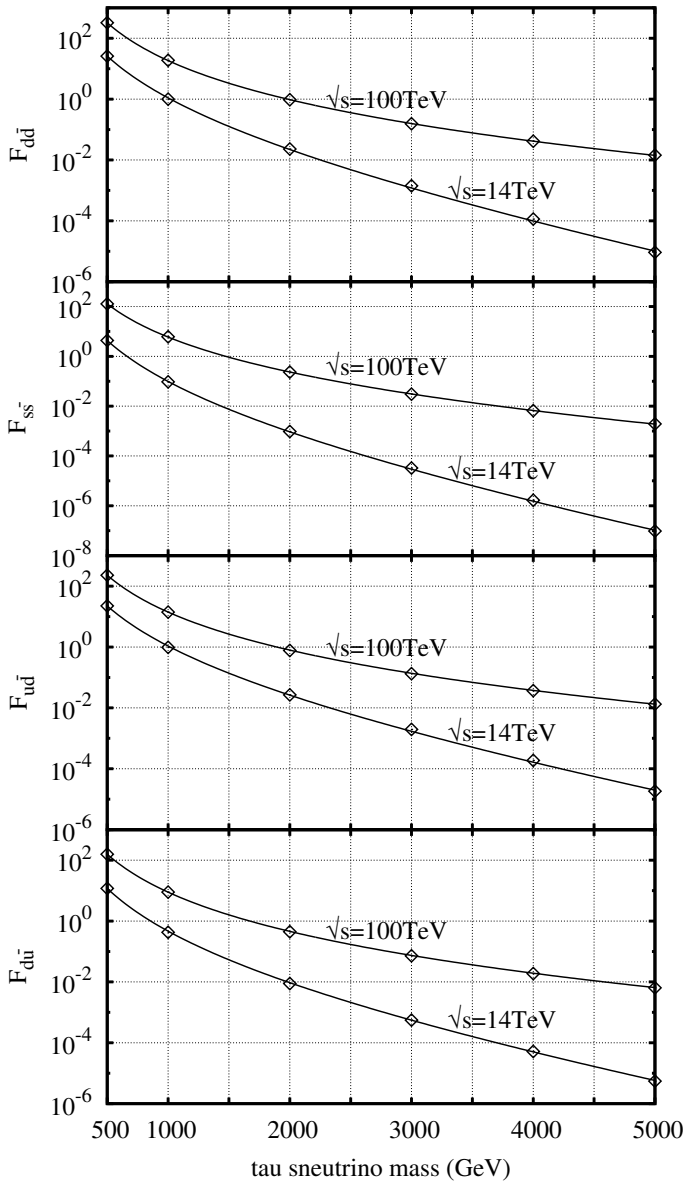

Figure 3: Fit functions and numerical results of $F(\sqrt{s}, m_{\tilde{\nu}_\tau}, q_1, q_2)$ for collision energy $\sqrt{s} = 14$TeV and $\sqrt{s} = 100$TeV. Rotated squares are numerical results calculated from Eq. (23), and lines are fit functions.

as follows[3],

$$\begin{aligned}\sigma(pp \to jj) = &\frac{9}{16\pi}\Big\{F_{d\bar{d}} + F_{u\bar{d}} + F_{\bar{u}d}\Big\} m_{\tilde{\nu}_\tau} \times \frac{\lambda'^4_{311}}{3\lambda'^2_{311} + 3\lambda'^2_{322} + 4\lambda^2_{312} + 4\lambda^2_{321}} \\ &+ \frac{9}{16\pi}\Big\{F_{d\bar{d}} + F_{u\bar{d}} + F_{\bar{u}d} + F_{s\bar{s}}\Big\} m_{\tilde{\nu}_\tau} \times \frac{\lambda'^2_{311}\lambda'^2_{322}}{3\lambda'^2_{311} + 3\lambda'^2_{322} + 4\lambda^2_{312} + 4\lambda^2_{321}} \\ &+ \frac{9}{16\pi}\Big\{F_{s\bar{s}}\Big\} m_{\tilde{\nu}_\tau} \times \frac{\lambda'^4_{322}}{3\lambda'^2_{311} + 3\lambda'^2_{322} + 4\lambda^2_{312} + 4\lambda^2_{321}}.\end{aligned} \tag{26}$$

The terms of $F_{u\bar{d}}$ and $F_{\bar{u}d}$ are the left-handed stau exchange contributions. Since the tau sneutrino

[3]Both the s-channel and t-channel $\tilde{\nu}_{\tau_L}$ ($\tilde{\tau}_L$) exchange processes contribute the dijet production in our scenario. Since the s-channel processes are highly dominant, we can formulate $\sigma(pp \to jj)$ with the Breit-Wigner formula.

and the stau are component of the $SU(2)_L$ doublet, we assumed their degeneracy in mass. In the case 1 (case 2), only the first line (third line) contributes to the dijet production.

3.3 NSI

With the interaction Eq. (3), there is modification on neutrino oscillation physics. It is called Non-Standard Interaction (NSI). Particularly, there is a strong enhancement, called chiral enhancement.

Conventional beam experiments use neutrino emitted by π decay. In the presence of the interaction Eq. (3), we have an effective operator which causes a π decay with LFV in the follwing way.

The effective Lagrangian is

$$\mathcal{L} = \frac{2\lambda^*_{312}\lambda'_{311}}{m^2_{\tilde{\tau}}}\bar{\nu}_e\mu_R\bar{d}_R u_L + \frac{2\lambda^*_{321}\lambda'_{311}}{m^2_{\tilde{\tau}}}\bar{\nu}_\mu e_R\bar{d}_R u_L + \text{h.c.}. \tag{27}$$

Amplitude for $\pi^+ \to \mu^+\nu_e$ is proportional to

$$\mathcal{M} \propto < \nu_e\mu^+|\bar{\nu}_e\mu_R|0 >< 0|\bar{d}_R u_L|\pi^+ > . \tag{28}$$

Since [27]

$$\bar{d}_R u_L = \frac{i}{m}\partial_\mu(\bar{u}\gamma^\mu\gamma_5 d) \tag{29}$$

using equation of motion and $m = m_u + m_d$, a sum of u- and d- quark masses. Therefore the magnitude of the amplitude is enhanced by [28]

$$\frac{m^2_\pi}{m_\mu m} \tag{30}$$

comparing with usual current-current interaction. Here m_π is π mass. This is the chiral enhancement. We can expect 30 times enhancement. It interferes with the usual π decay though it depends on the phase of $\lambda^*_{312}\lambda'_{311}$, and can affect the neutrino oscillation experiment with conventional beam.

The strength of the NSIs is parameterized by the relative strength with the weak interaction. For the conventional beam experiment the effect of $\pi^+ \to \mu^+\nu_e$ is denoted by $\epsilon^S_{\mu e}$ and

$$\epsilon^S_{\mu e} = \sqrt{2}\frac{m^2_\pi}{m_\mu m}\frac{2\lambda^*_{312}\lambda'_{311}}{G_F m^2_{\tilde{\tau}}}. \tag{31}$$

With this interaction, the μ flavor eigenstate in the π decay , which is denoted by $(0, 1, 0)$ in the lepton flavor eigenstates, is deformed to be $(\epsilon^S_{\mu e}, 1, 0)$.

Note that the operator $\bar{e}_R\nu_\mu\bar{u}_L d_R$ causes $\pi^- \to e^-\bar{\nu}_\mu$. It has an electron final state. Since there is μ in π decay more than 99% case it cannot interfere with a usual π decay and hence it has no effect on neutrino oscillation experiment. Furthermore π decay cannot be caused by operators with λ'_{322}. It means, in principle, with neutrino oscillation experiment operator with $\lambda^*_{312}\lambda'_{311}$ can be distinguished from others.

In principle, there are other NSI processes in matter effect and detection process. They are, however, absent or tiny. Indeed there is no matter effect as λ_{311} is absent. The NSI effect detection process is suppressed by chirality since the interaction is not (V-A)(V-A) type [29].

Table 3: Current and future experimental limits on the μ-e conversion branching ratio and the upper limits on $\lambda'\lambda$ corresponding to each experimental limit.

Experiment	BR limit	Limit on $\lambda'_{311}\lambda$ (case-I)	Limit on $\lambda'_{322}\lambda$ (case-II)	Limit on $\lambda'\lambda$ (case-III)
SINDRUM	7×10^{-13} [4]	$1.633\times10^{-7}\left(\frac{m_{\tilde{\nu}_\tau}}{1\text{TeV}}\right)^2$	$3.170\times10^{-7}\left(\frac{m_{\tilde{\nu}_\tau}}{1\text{TeV}}\right)^2$	$1.072\times10^{-7}\left(\frac{m_{\tilde{\nu}_\tau}}{1\text{TeV}}\right)^2$
DeeMe	5×10^{-15} [15]	$1.550\times10^{-8}\left(\frac{m_{\tilde{\nu}_\tau}}{1\text{TeV}}\right)^2$	$2.915\times10^{-8}\left(\frac{m_{\tilde{\nu}_\tau}}{1\text{TeV}}\right)^2$	$1.012\times10^{-8}\left(\frac{m_{\tilde{\nu}_\tau}}{1\text{TeV}}\right)^2$
COMET-I	7×10^{-15} [14]	$1.830\times10^{-8}\left(\frac{m_{\tilde{\nu}_\tau}}{1\text{TeV}}\right)^2$	$3.504\times10^{-8}\left(\frac{m_{\tilde{\nu}_\tau}}{1\text{TeV}}\right)^2$	$1.196\times10^{-8}\left(\frac{m_{\tilde{\nu}_\tau}}{1\text{TeV}}\right)^2$
COMET-II	3×10^{-17} [14]	$1.198\times10^{-9}\left(\frac{m_{\tilde{\nu}_\tau}}{1\text{TeV}}\right)^2$	$2.294\times10^{-9}\left(\frac{m_{\tilde{\nu}_\tau}}{1\text{TeV}}\right)^2$	$7.827\times10^{-10}\left(\frac{m_{\tilde{\nu}_\tau}}{1\text{TeV}}\right)^2$
PRISM	7×10^{-19} [14]	$1.830\times10^{-10}\left(\frac{m_{\tilde{\nu}_\tau}}{1\text{TeV}}\right)^2$	$3.504\times10^{-10}\left(\frac{m_{\tilde{\nu}_\tau}}{1\text{TeV}}\right)^2$	$1.196\times10^{-10}\left(\frac{m_{\tilde{\nu}_\tau}}{1\text{TeV}}\right)^2$

3.4 Muonium conversion

In the scenario, muonium ($M=\mu^+e^-$) converts to autimuonium ($\bar{M}=\mu^-e^+$) via the tau sneutrino exchange. The M-$\bar{M}$ conversion is described by $(V\pm A)\times(V\pm A)$ form interaction [30]

$$\mathcal{L}(M\to\bar{M})=\frac{G_{M\bar{M}}}{\sqrt{2}}(\bar{\mu}\gamma_\mu P_L e)(\bar{\mu}\gamma^\mu P_R e)+\text{h.c.}. \tag{32}$$

Here $G_{M\bar{M}}$ is an effective coupling analogous to the Fermi coupling constant G_F. Latest experimental limit of M-$\bar{M}$ conversion is set on the $G_{M\bar{M}}$, $G_{M\bar{M}}\leq 3.0\times10^{-3}G_F$ [31]. We derive the interaction Lagrangian describing the M-$\bar{M}$ conversion by the Fierz transformation from the fundamental Lagrangian (3) as follows,

$$\mathcal{L}(M\to\bar{M})=\frac{\lambda_{321}\lambda^*_{312}}{2m^2_{\tilde{\nu}_\tau}}(\bar{\mu}\gamma_\mu P_L e)(\bar{\mu}\gamma^\mu P_R e)+\text{h.c.}. \tag{33}$$

Thus the upper bound from M-$\bar{M}$ conversion search experiment is

$$|\lambda_{321}\lambda^*_{312}|\left(\frac{1\text{TeV}}{m_{\tilde{\nu}_\tau}}\right)^2\leq 4.948\times10^{-2}. \tag{34}$$

4 Numerical result

We are now in a position to show numerical results. Table 3 shows the current experimental limit and the future single event sensitivity for μ-e conversion process, and shows the upper limits on the combination of the RPV couplings, $\lambda'\lambda$, corresponding to the limit and the sensitivities in each experiment. In the calculation of the upper limits, we take Au, Si, and Al for target nucleus of SINDRUM-II, DeeMe, and other experiments, respectively.

μ-e conversion search is a reliable probe to both the RPV couplings and tau sneutrino mass. The current experimental limit puts strict limit on the RPV couplings, $\lambda'\lambda\lesssim10^{-7}$ for $m_{\tilde{\nu}_\tau}=1$TeV and $\lambda'\lambda\lesssim10^{-5}$ for $m_{\tilde{\nu}_\tau}=3$TeV, respectively. In near future, the accessible RPV couplings will be extended by more than 3 orders of current limits, $\lambda'\lambda\simeq10^{-10}$ for $m_{\tilde{\nu}_\tau}=1$TeV and $\lambda'\lambda\simeq10^{-8}$ for $m_{\tilde{\nu}_\tau}=3$TeV, respectively.

The μ-e conversion process is one of the clear signatures for the RPV scenario, but it is not the sufficient evidence of the scenario. We must check the correlations among the reaction rates

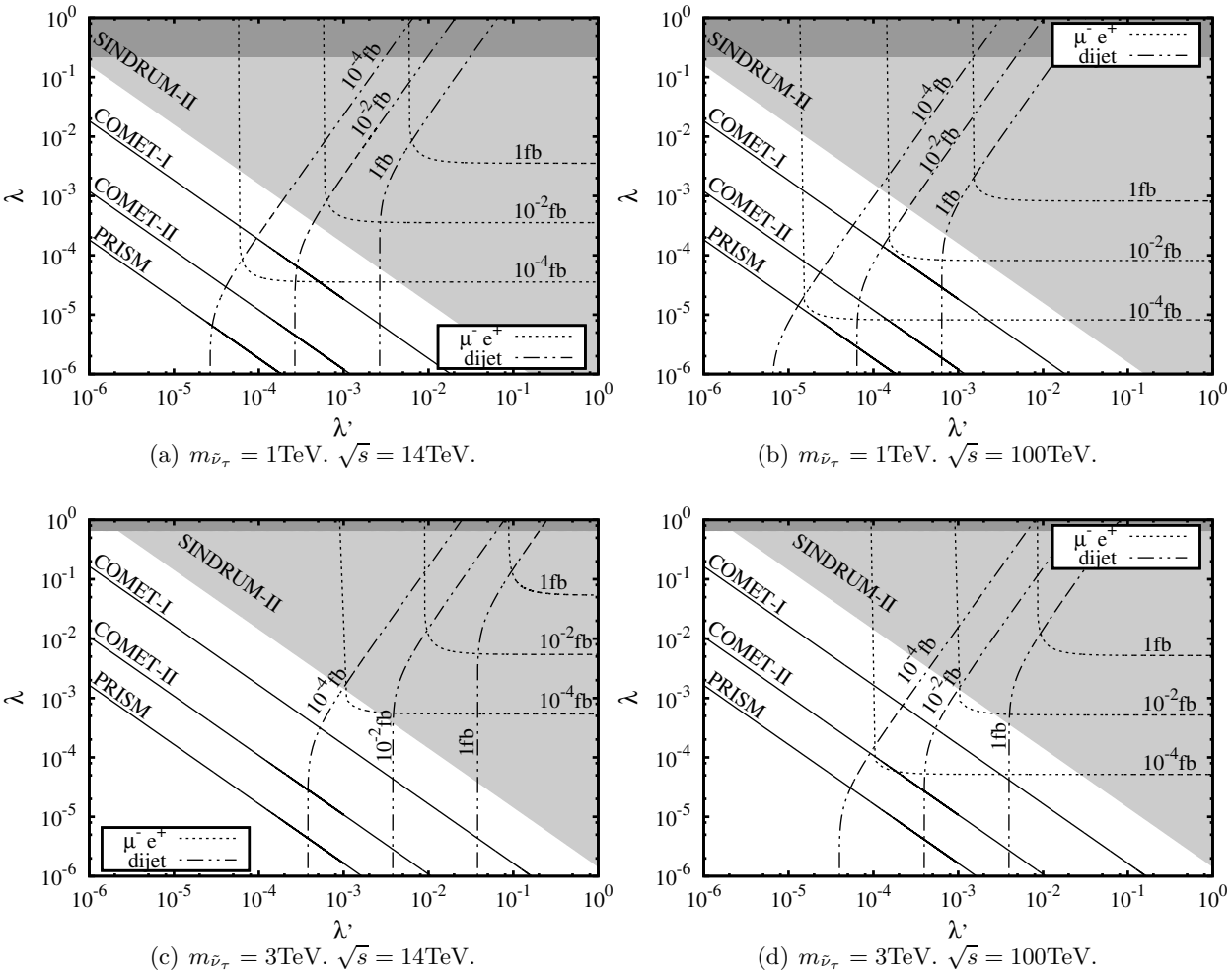

(a) $m_{\tilde{\nu}_\tau} = 1$TeV. $\sqrt{s} = 14$TeV. (b) $m_{\tilde{\nu}_\tau} = 1$TeV. $\sqrt{s} = 100$TeV.

(c) $m_{\tilde{\nu}_\tau} = 3$TeV. $\sqrt{s} = 14$TeV. (d) $m_{\tilde{\nu}_\tau} = 3$TeV. $\sqrt{s} = 100$TeV.

Figure 4: Contour plot of $\sigma(pp \to \mu^- e^+)$, $\sigma(pp \to dijet)$, and BR$(\mu^- N \to e^- N)$ in the case-I for (a) $m_{\tilde{\nu}_\tau} = 1$TeV and $\sqrt{s} = 14$TeV (b) $m_{\tilde{\nu}_\tau} = 1$TeV and $\sqrt{s} = 100$TeV (c) $m_{\tilde{\nu}_\tau} = 3$TeV and $\sqrt{s} = 14$TeV (d) $m_{\tilde{\nu}_\tau} = 3$TeV and $\sqrt{s} = 100$TeV. For simplicity, we take universal RPV coupling, $\lambda \equiv \lambda_{312} = \lambda_{321} = -\lambda_{132} = -\lambda_{231}$. Light shaded region is excluded by the μ-e conversion search [4], and dark shaded band is excluded region by the M-$\bar{M}$ conversion search [31].

of μ-e conversion process, the cross sections of $pp \to \mu^- e^+$ and $pp \to jj$, and so on in order to discriminate the case-I, -II, and -III each other and to confirm the RPV scenario. In the following subsections, in each case, we show the correlations, and discuss the parameter determination.

4.1 Case-I ($\lambda'_{311} \neq 0$, $\lambda'_{322} = 0$)

The parameter dependence of $\sigma(pp \to \mu^- e^+)$, $\sigma(pp \to jj)$, and BR$(\mu^- N \to e^- N)$ are depicted in Fig. 4. Dashed and dot-dashed lines are contours of $\sigma(pp \to \mu^- e^+)$ and $\sigma(pp \to jj)$ at $\sqrt{s} = 14$TeV (left panels) and $\sqrt{s} = 100$TeV (right panels), respectively. Solid lines are contours of BR$(\mu^-\mathrm{Al} \to e^-\mathrm{Al})$, which are translated from the single event sensitivities of each experiments (see Table 3). Light shaded region is excluded by the μ-e conversion search at the SINDRUM-II experiment [4], and dark shaded band is excluded region by the M-$\bar{M}$ conversion search experiment at the Paul Scherrer Institute (PSI) [31]. We take $m_{\tilde{\nu}_\tau} = 1$TeV for panels (a) and (b), and $m_{\tilde{\nu}_\tau} = 3$TeV for panels (c) and (d). For simplicity, we take the couplings universally in leptonic

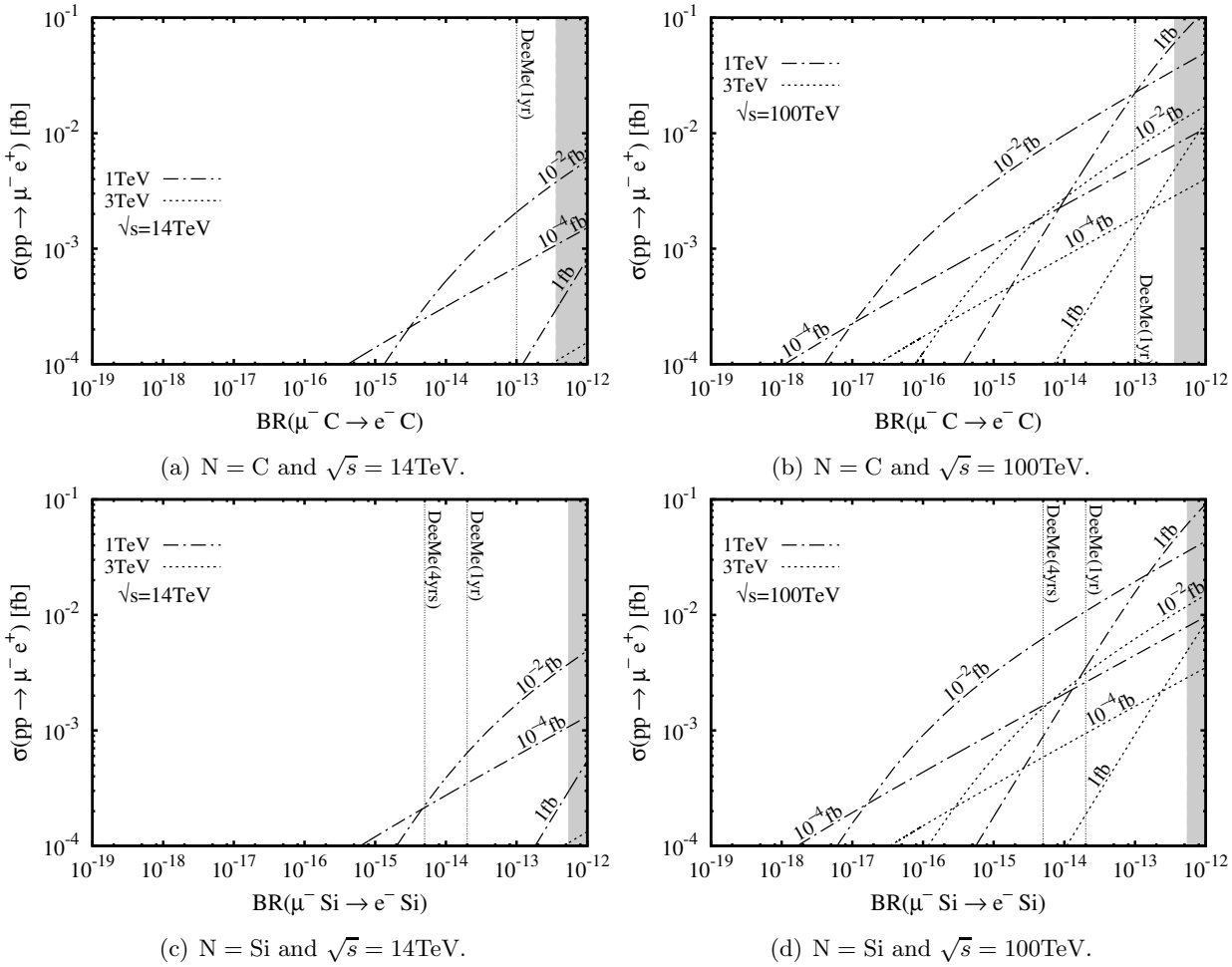

(a) N = C and $\sqrt{s} = 14$TeV.

(b) N = C and $\sqrt{s} = 100$TeV.

(c) N = Si and $\sqrt{s} = 14$TeV.

(d) N = Si and $\sqrt{s} = 100$TeV.

Figure 5: $\sigma(pp \to \mu^- e^+)$ as a function of BR$(\mu^- N \to e^- N)$ for each $\sigma(pp \to jj)$ in the case-I. $\sigma(pp \to jj)$ are attached on each line. Results for $m_{\tilde{\nu}_\tau} = 1$TeV ($m_{\tilde{\nu}_\tau} = 3$TeV) are given by dot-dashed line (dotted line). Shaded region in each panel is the excluded region by the SINDRUM-I I experiment. Left panels show the results for the collision energy $\sqrt{s} = 14$TeV, and right panels show the results for $\sqrt{s} = 100$TeV. We take C [(a) and (b)], and Si [(c) and (d)] for the target nucleus of μ-e conversion process.

RPV sector: $\lambda \equiv \lambda_{312} = \lambda_{321} = -\lambda_{132} = -\lambda_{231}$.

Figure 4 displays the strong potential of μ-e conversion search to explore the RPV scenarios. The PRISM experiment will cover almost parameter space wherein the LHC experiment can survey. In the parameter range between the SINDRUM-Ⅱ limit and the PRISM reach, combining the measurement results of $\sigma(pp \to \mu^- e^+)$, $\sigma(pp \to jj)$, and BR$(\mu^-\text{Al} \to e^-\text{Al})$, the RPV couplings and the tau sneutrino mass will be precisely determined.

Figures 5 and 6 show $\sigma(pp \to \mu\bar{e})$ as a function of BR$(\mu + N \to e + N)$ in the case-I. Candidate materials for the target of μ-e conversion search are carbon (C) and silicon (Si) at the DeeMe experiment, and are aluminum (Al) or titanium (Ti) at the COMET, Mu2e, and PRISM experiment. Vertical dotted lines show the experimental reach of DeeMe 1-year running (DeeMe(1yr)), DeeMe 4-years running (DeeMe(4yrs)), COMET phase-I (COMET-I), COMET phase-Ⅱ (COMET-Ⅱ), and PRISM (PRISM). Shaded regions are the excluded region by the

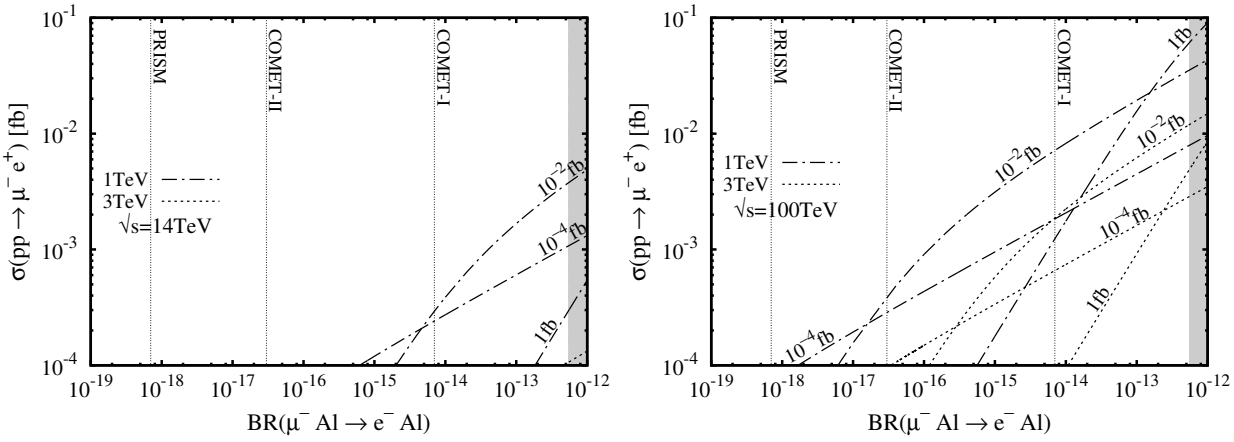

(a) N = Al and $\sqrt{s} = 14$TeV.

(b) N = Al and $\sqrt{s} = 100$TeV.

(c) N = Ti and $\sqrt{s} = 14$TeV.

(d) N = Ti and $\sqrt{s} = 100$TeV.

Figure 6: Same as Fig. 5 except for target nucleus. We take Al [(a) and (b)], and Ti [(c) and (d)] for the target nucleus of μ-e conversion process.

SINDRUM-II experiment [4], which are translated into the limit for each nucleus from that for Au. The experimental reach of Mu2e experiment is planned to be similar of the COMET phase-II [32]. Left and right panels show the results of $\sqrt{s} = 14$TeV and $\sqrt{s} = 100$TeV, respectively. Results for $m_{\tilde{\nu}_\tau} = 1$TeV and $m_{\tilde{\nu}_\tau} = 3$TeV are given by dot-dashed line and dotted line, respectively. Each line corresponds to the dijet production cross section at the LHC, $\sigma(pp \to jj)$, at $\sqrt{s} = 14$TeV (left panels) and at $\sqrt{s} = 100$TeV (right panels), respectively. For simplicity, we take universal RPV coupling, $\lambda \equiv \lambda_{312} = \lambda_{321} = -\lambda_{132} = -\lambda_{231}$.

Figures 5 and 6 show the clear correlations among $\sigma(pp \to \mu^- e^+)$, $\sigma(pp \to jj)$, and BR($\mu^- N \to e^- N$). Checking the correlations makes possible to distinguish the RPV scenario and other new physics scenarios.

In Figs 5 and 6, behavior of the correlations are not so intuitive. We quantitatively analyze the behavior. We infer the $\sigma(pp \to \mu^- e^+)$ from the $\sigma(pp \to jj)$ and BR($\mu^- N \to e^- N$).

As we formulated in Secs. 3.1 and 3.2, BR $\equiv$ BR($\mu^- N \to e^- N$) and $\sigma_{jet} \equiv \sigma(pp \to jj)$ are divided into the kinematics part and RPV coupling dependent part as follows,

$$\text{BR} = k_N (\lambda'_{311} \lambda)^2, \tag{35}$$

Table 4: Numerical value of k_N for a target nucleus N in each case.

	C	Al	Si	Ti	Au
case-I	$13.83\left(\frac{1\text{TeV}}{m_{\tilde{\nu}_\tau}}\right)^4$	$20.92\left(\frac{1\text{TeV}}{m_{\tilde{\nu}_\tau}}\right)^4$	$20.80\left(\frac{1\text{TeV}}{m_{\tilde{\nu}_\tau}}\right)^4$	$35.71\left(\frac{1\text{TeV}}{m_{\tilde{\nu}_\tau}}\right)^4$	$26.26\left(\frac{1\text{TeV}}{m_{\tilde{\nu}_\tau}}\right)^4$
case-II	$3.913\left(\frac{1\text{TeV}}{m_{\tilde{\nu}_\tau}}\right)^4$	$5.881\left(\frac{1\text{TeV}}{m_{\tilde{\nu}_\tau}}\right)^4$	$5.886\left(\frac{1\text{TeV}}{m_{\tilde{\nu}_\tau}}\right)^4$	$9.962\left(\frac{1\text{TeV}}{m_{\tilde{\nu}_\tau}}\right)^4$	$7.185\left(\frac{1\text{TeV}}{m_{\tilde{\nu}_\tau}}\right)^4$
case-III	$32.46\left(\frac{1\text{TeV}}{m_{\tilde{\nu}_\tau}}\right)^4$	$48.97\left(\frac{1\text{TeV}}{m_{\tilde{\nu}_\tau}}\right)^4$	$48.83\left(\frac{1\text{TeV}}{m_{\tilde{\nu}_\tau}}\right)^4$	$83.38\left(\frac{1\text{TeV}}{m_{\tilde{\nu}_\tau}}\right)^4$	$60.91\left(\frac{1\text{TeV}}{m_{\tilde{\nu}_\tau}}\right)^4$

$$\sigma_{jet} \equiv \sigma(pp \to jj) = F_{jet}\frac{\lambda'^4_{311}}{3\lambda'^2_{311} + 8\lambda^2}. \tag{36}$$

Here k_N is a coefficient depending on a target nucleus N and the sneutrino mass, which values are calculated by Eqs. (17)-(20) and are listed in Table 4. F_{jet} includes the numerical factor and kinematical factor in σ_{jet}, and is calculated from Eq. (26), $F_{jet} = \frac{9}{16\pi}\left\{F_{d\bar{d}} + F_{u\bar{d}} + F_{\bar{u}d}\right\} m_{\tilde{\nu}_\tau}$. We have a cubic equation of λ'^2_{311} from Eqs. (35) and (36),

$$k_N F_{jet}(\lambda'^2_{311})^3 - 3k_N(\lambda'^2_{311})^2 - 8\sigma_{jet}\text{BR} = 0. \tag{37}$$

By solving the cubic equation, we obtain an analytic expression of λ'^2_{311} as a function of BR,

$$\begin{aligned}\lambda'^2_{311} = &\left\{\left(\frac{2\sigma_{jet}\text{BR}}{k_N F_{jet}}\right) + \left(\frac{\sigma_{jet}}{F_{jet}}\right)^3 + \sqrt{\left(\frac{2\sigma_{jet}\text{BR}}{k_N F_{jet}} + \left(\frac{\sigma_{jet}}{F_{jet}}\right)^3\right)^2 - \left(\frac{\sigma_{jet}}{F_{jet}}\right)^6}\right\}^{1/3} \\ &+ \left\{\left(\frac{2\sigma_{jet}\text{BR}}{k_N F_{jet}}\right) + \left(\frac{\sigma_{jet}}{F_{jet}}\right)^3 - \sqrt{\left(\frac{2\sigma_{jet}\text{BR}}{k_N F_{jet}} + \left(\frac{\sigma_{jet}}{F_{jet}}\right)^3\right)^2 - \left(\frac{\sigma_{jet}}{F_{jet}}\right)^6}\right\}^{1/3} \\ &+ \frac{\sigma_{jet}}{F_{jet}}.\end{aligned} \tag{38}$$

λ^2 is easily obtained from Eqs. (35) and (38),

$$\begin{aligned}\lambda^2 &= \frac{\text{BR}}{k_N \lambda'^2_{311}} \\ &= \frac{\text{BR}}{k_N}\left\{\frac{\sigma_{jet}}{F_{jet}} + \left[\left(\frac{2\sigma_{jet}\text{BR}}{k_N F_{jet}}\right) + \left(\frac{\sigma_{jet}}{F_{jet}}\right)^3 + \sqrt{\left(\frac{2\sigma_{jet}\text{BR}}{k_N F_{jet}} + \left(\frac{\sigma_{jet}}{F_{jet}}\right)^3\right)^2 - \left(\frac{\sigma_{jet}}{F_{jet}}\right)^6}\right]^{1/3}\right. \\ &\quad \left. + \left[\left(\frac{2\sigma_{jet}\text{BR}}{k_N F_{jet}}\right) + \left(\frac{\sigma_{jet}}{F_{jet}}\right)^3 - \sqrt{\left(\frac{2\sigma_{jet}\text{BR}}{k_N F_{jet}} + \left(\frac{\sigma_{jet}}{F_{jet}}\right)^3\right)^2 - \left(\frac{\sigma_{jet}}{F_{jet}}\right)^6}\right]^{1/3}\right\}^{-1}.\end{aligned} \tag{39}$$

As a result, by substituting λ'^2_{311} and λ^2 into the expression of $\sigma(pp \to \mu^- e^+)$ [Eq. (25)], we obtain the prediction of $\sigma(pp \to \mu^- e^+)$ as a function of BR and σ_{jet},

$$\sigma(pp \to \mu^- e^+) = \frac{12}{16\pi}F_{d\bar{d}} m_{\tilde{\nu}_\tau}\frac{(\text{BR}/k_N)}{3\lambda'^2_{311} + 8\lambda^2}. \tag{40}$$

Once σ_{jet} is measured, we can evaluate $\sigma(pp \to \mu^- e^+)$ as a function of BR with the Eq. (40). Note that the solution Eqs. (38) and (39) is uniquely determined as read in Fig. 4, and hence

$\sigma(pp \to \mu^- e^+)$ is also uniquely inferred. We cannot, however, determine σ_{jet} uniquely from BR and $\sigma(pp \to \mu^- e^+)$ since as a function of BR the latter is two-valued function as is n in Fig. 4. Therefore there are crosses of two lines in Figs. 5 and 6.

We quantitatively analyze the behavior for 2 reference points. As a first reference point, we take $N = \mathrm{Al}$, $m_{\tilde{\nu}_\tau} = 1\mathrm{TeV}$, $\sqrt{s} = 100\mathrm{TeV}$, and $\sigma_{jet} = 1\mathrm{fb}$. In this point, when $\mathrm{BR} \lesssim 10^{-13}$, λ'^2_{311} and λ^2 are approximately calculated from Eqs. (38) and (39) as follows,

$$\lambda'^2_{311} \simeq 3\left(\frac{\sigma_{jet}}{F_{jet}}\right), \quad \lambda^2 = \frac{\mathrm{BR}}{k_{\mathrm{Al}}\lambda'^2_{311}} = \frac{\mathrm{BR}}{3k_{\mathrm{Al}}}\left(\frac{F_{jet}}{\sigma_{jet}}\right). \tag{41}$$

By substituting λ'^2_{311} and λ^2 into Eq. (25), we obtain the approximate expression of $\sigma(pp \to \mu^- e^+)$, and find the BR dependence on $\sigma(pp \to \mu^- e^+)$ as follows,

$$\begin{aligned}\sigma(pp \to \mu^- e^+) &\simeq \frac{12}{16\pi} F_{d\bar{d}} m_{\tilde{\nu}_\tau} \frac{\mathrm{BR}/k_{\mathrm{Al}}}{3\cdot 3\left(\frac{\sigma_{jet}}{F_{jet}}\right) + 8\cdot\frac{\mathrm{BR}}{3k_{Al}}\left(\frac{F_{jet}}{\sigma_{jet}}\right)} \\ &\simeq \frac{1}{12\pi} F_{d\bar{d}} m_{\tilde{\nu}_\tau}\left(\frac{F_{jet}}{\sigma_{jet}k_{\mathrm{Al}}}\right)\mathrm{BR}.\end{aligned} \tag{42}$$

The BR dependence is consistent with the numerical result in Fig. 6. As a second reference point, we take $N = \mathrm{Al}$, $m_{\tilde{\nu}_\tau} = 1\mathrm{TeV}$, $\sqrt{s} = 100\mathrm{TeV}$, and $\sigma_{jet} = 10^{-4}\mathrm{fb}$. In this point, when $\mathrm{BR} \gtrsim 10^{-21}$, λ'^2_{311} and λ^2 are approximately calculated from Eqs. (38) and (39) as follows,

$$\lambda'^2_{311} \simeq 4\left(\frac{\sigma_{jet}\mathrm{BR}}{k_{\mathrm{Al}}F_{jet}}\right)^{1/3}, \quad \lambda^2 = \frac{\mathrm{BR}}{k_{\mathrm{Al}}\lambda'^2_{311}} = \frac{1}{4}\left(\frac{(\mathrm{BR})^2 F_{jet}}{k^2_{\mathrm{Al}}\sigma_{jet}}\right)^{1/3}. \tag{43}$$

By substituting λ'^2_{311} and λ^2 into Eq. (25), we obtain the approximate expression of $\sigma(pp \to \mu^- e^+)$, and find the BR dependence on $\sigma(pp \to \mu^- e^+)$ as follows,

$$\begin{aligned}\sigma(pp \to \mu^- e^+) &\simeq \frac{12}{16\pi} F_{d\bar{d}} m_{\tilde{\nu}_\tau} \frac{\mathrm{BR}/k_{\mathrm{Al}}}{3\cdot 4\left(\frac{\sigma_{jet}\mathrm{BR}}{k_{\mathrm{Al}}F_{jet}}\right)^{1/3} + 8\cdot\frac{1}{4}\left(\frac{(\mathrm{BR})^2 F_{jet}}{k^2_{\mathrm{Al}}\sigma_{jet}}\right)^{1/3}} \\ &\simeq \frac{3}{8\pi} F_{d\bar{d}} m_{\tilde{\nu}_\tau}\left(\frac{\sigma_{jet}}{k_{\mathrm{Al}}F_{jet}}\right)^{1/3}(\mathrm{BR})^{1/3}.\end{aligned} \tag{44}$$

The BR dependence is consistent with the numerical result in Fig. 6. Also in other points, we can similarly check the BR dependence, and find its consistency.

In Figs. 5 and 6, in some regions of $\mathrm{BR}(\mu^- N \to e^- N)$, larger $\sigma(pp \to jj)$ suggests smaller $\sigma(pp \to \mu^- e^+)$. This strange relation is simply understood as follows. Large $\sigma(pp \to jj)$ for a fixed $\mathrm{BR}(\mu^- N \to e^- N)$ leads large λ'_{311} and small λ (see Eqs. (15) and (26)). In this case, as is shown in Eq. (40), $\sigma(pp \to \mu^- e^+) \propto 1/\lambda'^2_{311}$. Thus, in some regions, we find the strange relation. This is one of the unique relation in the RPV scenario. In other models, if mediator universally couples to both quarks and leptons, we will not find the difference between $\sigma(pp \to jj)$ and $\sigma(pp \to \mu^- e^+)$ (except for color factor). We can distinguish such models from the RPV scenarios by checking the unique relation.

4.2 Case-II ($\lambda'_{311} = 0$ and $\lambda'_{322} \neq 0$)

Figure 7 displays the parameter dependence of $\sigma(pp \to \mu^- e^+)$, $\sigma(pp \to jj)$, and $\mathrm{BR}(\mu^- \mathrm{Al} \to e^- \mathrm{Al})$ in the case-II. The description of Fig. 7 is same as that of Fig. 4. Figures 8 and 9 show

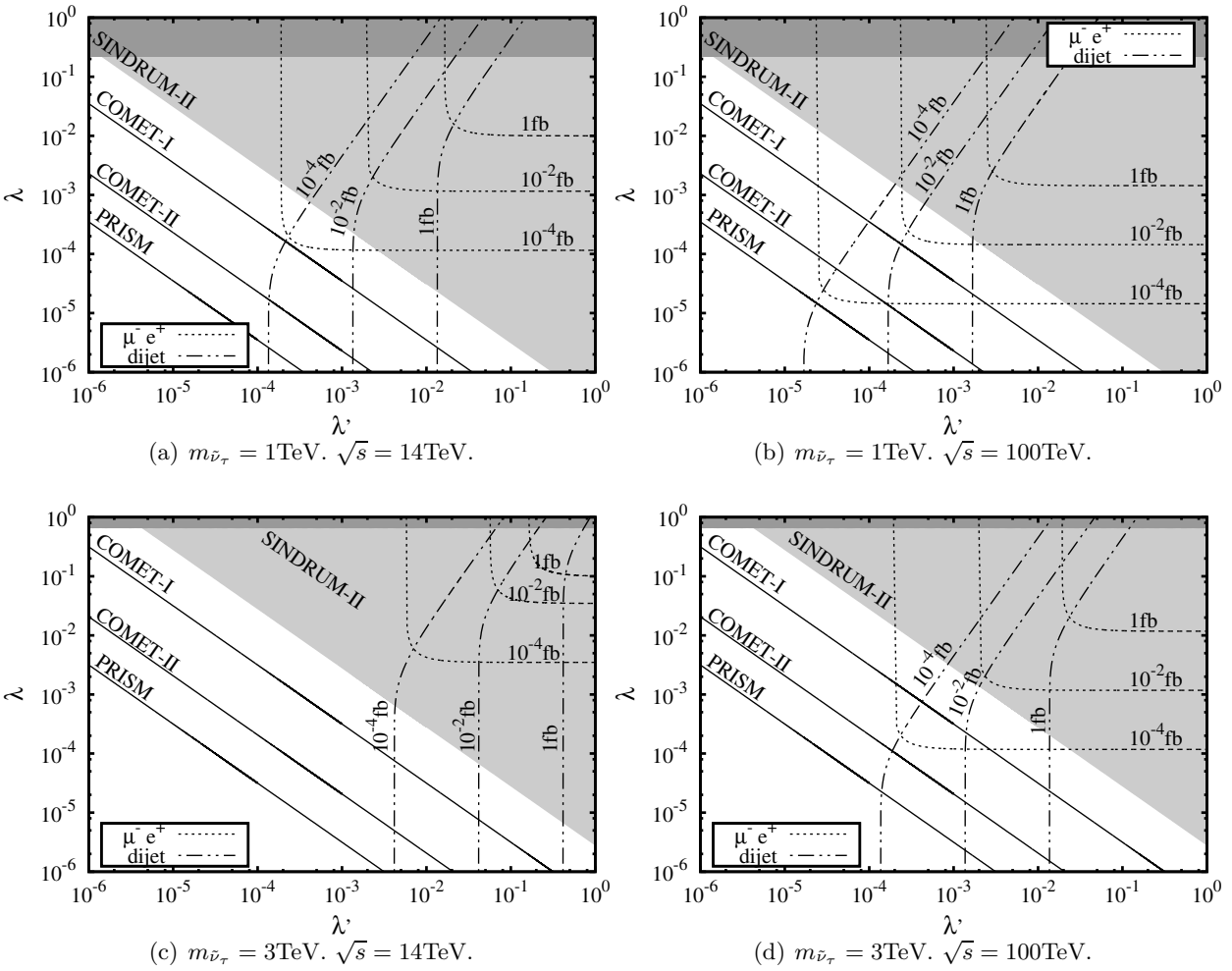

(a) $m_{\tilde{\nu}_\tau} = 1\text{TeV}$. $\sqrt{s} = 14\text{TeV}$. (b) $m_{\tilde{\nu}_\tau} = 1\text{TeV}$. $\sqrt{s} = 100\text{TeV}$.

(c) $m_{\tilde{\nu}_\tau} = 3\text{TeV}$. $\sqrt{s} = 14\text{TeV}$. (d) $m_{\tilde{\nu}_\tau} = 3\text{TeV}$. $\sqrt{s} = 100\text{TeV}$.

Figure 7: Contour plot of $\sigma(pp \to \mu^- e^+)$, $\sigma(pp \to jj)$, and $\text{BR}(\mu^- N \to e^- N)$ in the case-II for (a) $m_{\tilde{\nu}_\tau} = 1\text{TeV}$ and $\sqrt{s} = 14\text{TeV}$ (b) $m_{\tilde{\nu}_\tau} = 1\text{TeV}$ and $\sqrt{s} = 100\text{TeV}$ (c) $m_{\tilde{\nu}_\tau} = 3\text{TeV}$ and $\sqrt{s} = 14\text{TeV}$ (d) $m_{\tilde{\nu}_\tau} = 3\text{TeV}$ and $\sqrt{s} = 100\text{TeV}$. For simplicity, we take universal RPV coupling, $\lambda \equiv \lambda_{312} = \lambda_{321} = -\lambda_{132} = -\lambda_{231}$. Light shaded region is excluded by the μ-e conversion search [4], and dark shaded band is excluded region by the M-$\bar{M}$ conversion search [31].

$\sigma(pp \to \mu^- e^+)$ as a function of $\text{BR}(\mu^- \text{Al} \to e^- \text{Al})$ in the case-II. The descriptions of the figures are same as those of Figs. 5 and 6.

The RPV parameters are determined by measuring $\sigma(pp \to \mu^- e^+)$, $\sigma(pp \to jj)$, and $\text{BR}(\mu^- \text{Al} \to e^- \text{Al})$, and plot the point on Fig. 7. Since $\sigma(pp \to \mu^- e^+)$ at 14TeV LHC is too small for the parameter determination, we must focus on the invariant mass from dijet. Precise measurements both of the tau sneutrino mass and $\sigma(pp \to jj)$ specify a contour of $\sigma(pp \to jj)$ in λ'_{322}-λ plane. Then precise measurement of $\text{BR}(\mu^- \text{Al} \to e^- \text{Al})$ can pin down the right parameter set on the contour. The accuracy of the pin-down strongly depends on the accuracy both of the invariant mass reconstruction and measurement of $\text{BR}(\mu^- \text{Al} \to e^- \text{Al})$. We will discuss the issue in detail in a separate publication [33].

After the discovery of μ-e conversion signal, if the constructed invariant mass is heavier than 1TeV in measuring $pp \to \mu^- e^+$ and $pp \to jj$ at $\sqrt{s} = 14\text{TeV}$, the case-II is ruled out. In the case-I I, accessible parameter space at the LHC with $\sqrt{s} = 14\text{TeV}$ collision is limited to within the space

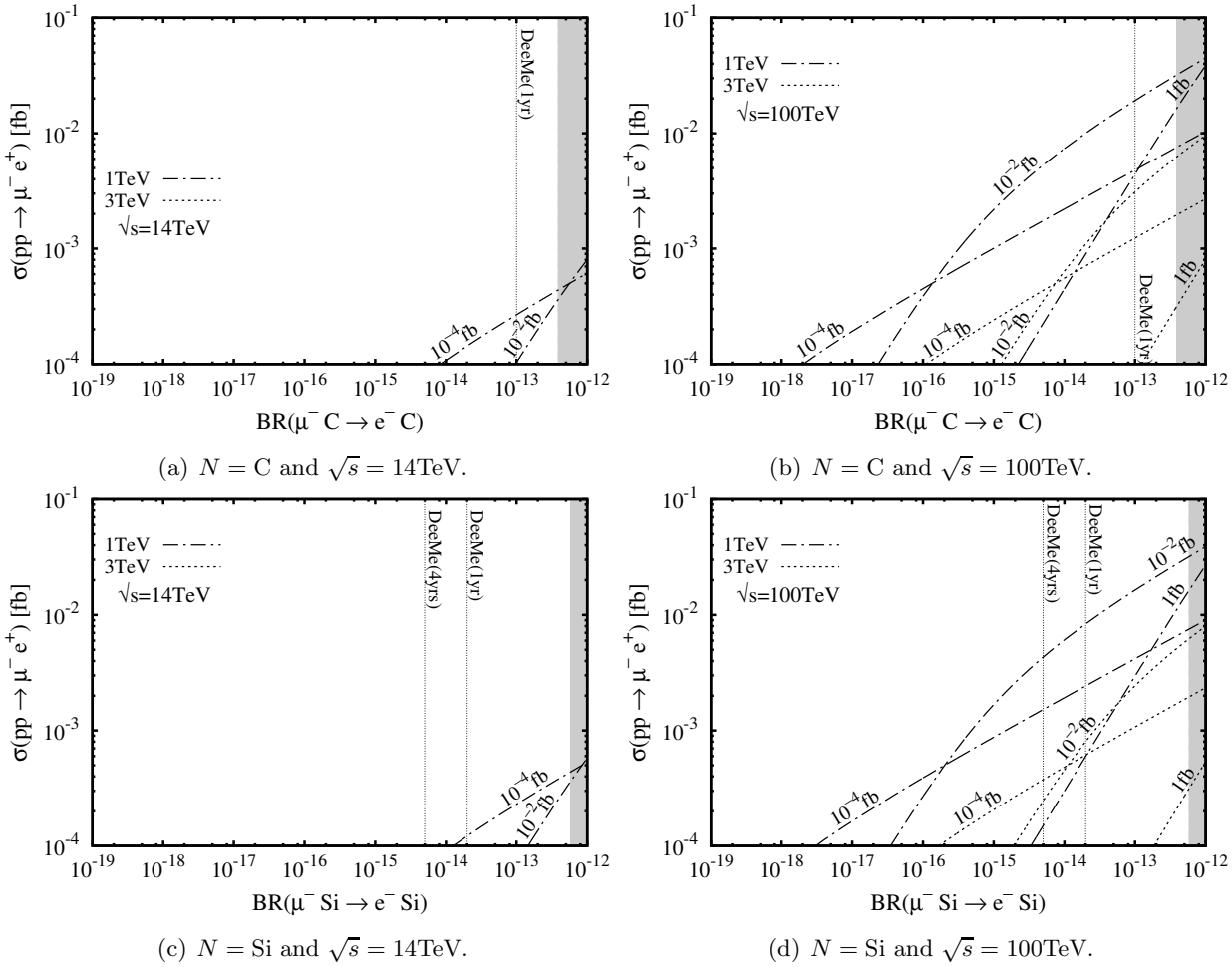

(a) $N = \mathrm{C}$ and $\sqrt{s} = 14\mathrm{TeV}$.

(b) $N = \mathrm{C}$ and $\sqrt{s} = 100\mathrm{TeV}$.

(c) $N = \mathrm{Si}$ and $\sqrt{s} = 14\mathrm{TeV}$.

(d) $N = \mathrm{Si}$ and $\sqrt{s} = 100\mathrm{TeV}$.

Figure 8: $\sigma(pp \to \mu^- e^+)$ as a function of $\mathrm{BR}(\mu^- N \to e^- N)$ for each $\sigma(pp \to jj)$ in the case-I I. $\sigma(pp \to jj)$ are attached on each line. Results for $m_{\tilde{\nu}_\tau} = 1\mathrm{TeV}$ ($m_{\tilde{\nu}_\tau} = 3\mathrm{TeV}$) are given by dot-dashed line (dotted line). Shaded regions are the excluded region by the SINDRUM-Ⅱ experiment. Left panels show the results for the collision energy $\sqrt{s} = 14\mathrm{TeV}$, and right panels show the results for $\sqrt{s} = 100\mathrm{TeV}$. We take C [(a) and (b)], and Si [(c) and (d)] for the target nucleus of μ-e conversion process.

for lighter tau sneutrino, $m_{\tilde{\nu}_\tau} \lesssim 1\mathrm{TeV}$. This is because both $\sigma(pp \to \mu^- e^+)$ and $\sigma(pp \to jj)$ are too small due to the low density of strange quark component in a proton (see Fig. 3). We need the 100TeV hadron collider to explore the parameter space for heavier sneutrino, $m_{\tilde{\nu}_\tau} \gtrsim 1\mathrm{TeV}$, in the case-Ⅱ.

Because of the low density of strange quark component in a proton, the reaction rate of μ-e conversion in case-Ⅱ is clearly different from that in case-I and -Ⅲ. For a fixed combination of $\sigma(pp \to \mu^- e^+)$ and $\sigma(pp \to jj)$, the expected $\mathrm{BR}(\mu^- N \to e^- N)$ is small compared with that in case-I and -Ⅲ (Eqs. (17) - (20)), and hence it is easy to discriminate case-Ⅱ scenario and case-I and -Ⅲ by checking the correlations in Figs. 8 and 9. It is important to emphasize that we have to exhibit the correlations in order for verification of RPV scenarios wherein cLFV processes will never be found except for μ-e conversion. It is first time that the correlations are graphically shown in RPV SUSY models.

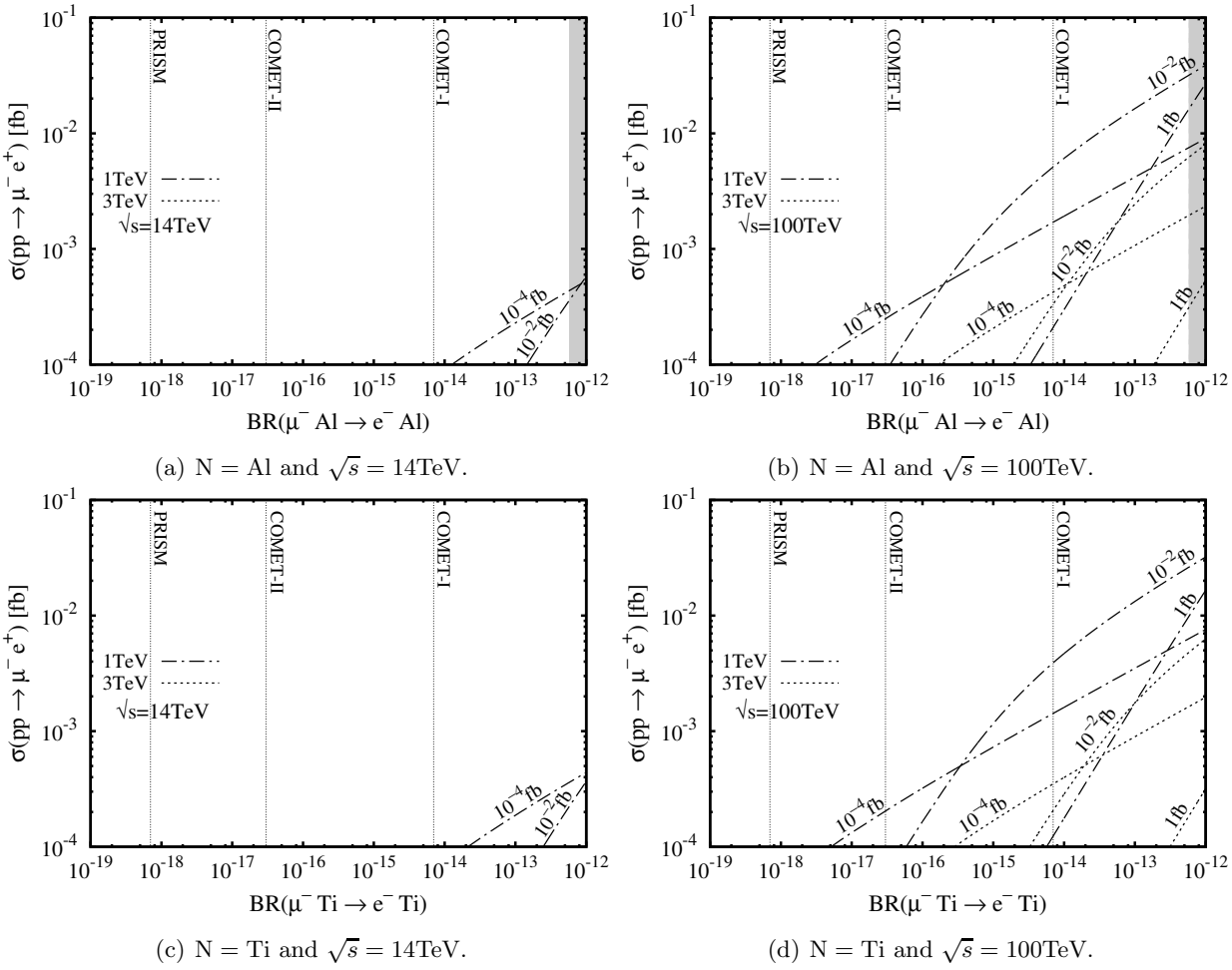

(a) N = Al and $\sqrt{s} = 14$TeV.

(b) N = Al and $\sqrt{s} = 100$TeV.

(c) N = Ti and $\sqrt{s} = 14$TeV.

(d) N = Ti and $\sqrt{s} = 100$TeV.

Figure 9: Same as Fig. 8 except for target nucleus. We take Al [(a) and (b)], and Ti [(c) and (d)] for the target nucleus of μ-e conversion process.

4.3 Case-III ($\lambda'_{311} \neq 0$ and $\lambda'_{322} \neq 0$)

Figure 10 displays the parameter dependence of $\sigma(pp \to \mu^- e^+)$, $\sigma(pp \to jj)$, and BR(μ^-Al $\to$ e^-Al) in the case-III. The description of Fig. 10 is same as that of Fig. 4. Figures 11 and 12 show $\sigma(pp \to \mu^- e^+)$ as a function of BR(μ^-Al $\to e^-$Al) in the case-III. The description of the figure is same as those of Figs. 5 and 6.

We can check the nice consistency between theoretical calculations and the behavior of plots in Figs. 11 and 12 by repeating the same quantitative analyze in Sec. 4.1 with F_{jet} and k_N for the case-III (see Table 4).

We can discriminate case-I, -II, and -III by checking the correlations of $\sigma(pp \to \mu^- e^+)$, $\sigma(pp \to jj)$, and BR(μ^-Al $\to e^-$Al) with Figs. 5, 6, 8, 9, 11, and 12. And, as we discussed in case-I and -I I, the RPV couplings are precisely determined via the measurement $\sigma(pp \to \mu^- e^+)$, $\sigma(pp \to jj)$, and BR(μ^-Al $\to e^-$Al) by using Fig. 10.

4.4 comment for NSI

In Figs 10, 11, and 12, for simplicity, we take $\lambda'_{311} = \lambda'_{322}$. When we take $\lambda'_{311} \neq \lambda'_{322}$, as is studied in Sec. 3.1 and Sec. 3.2, behavior of the plots are basically same with Figs 10, 11, and 12.

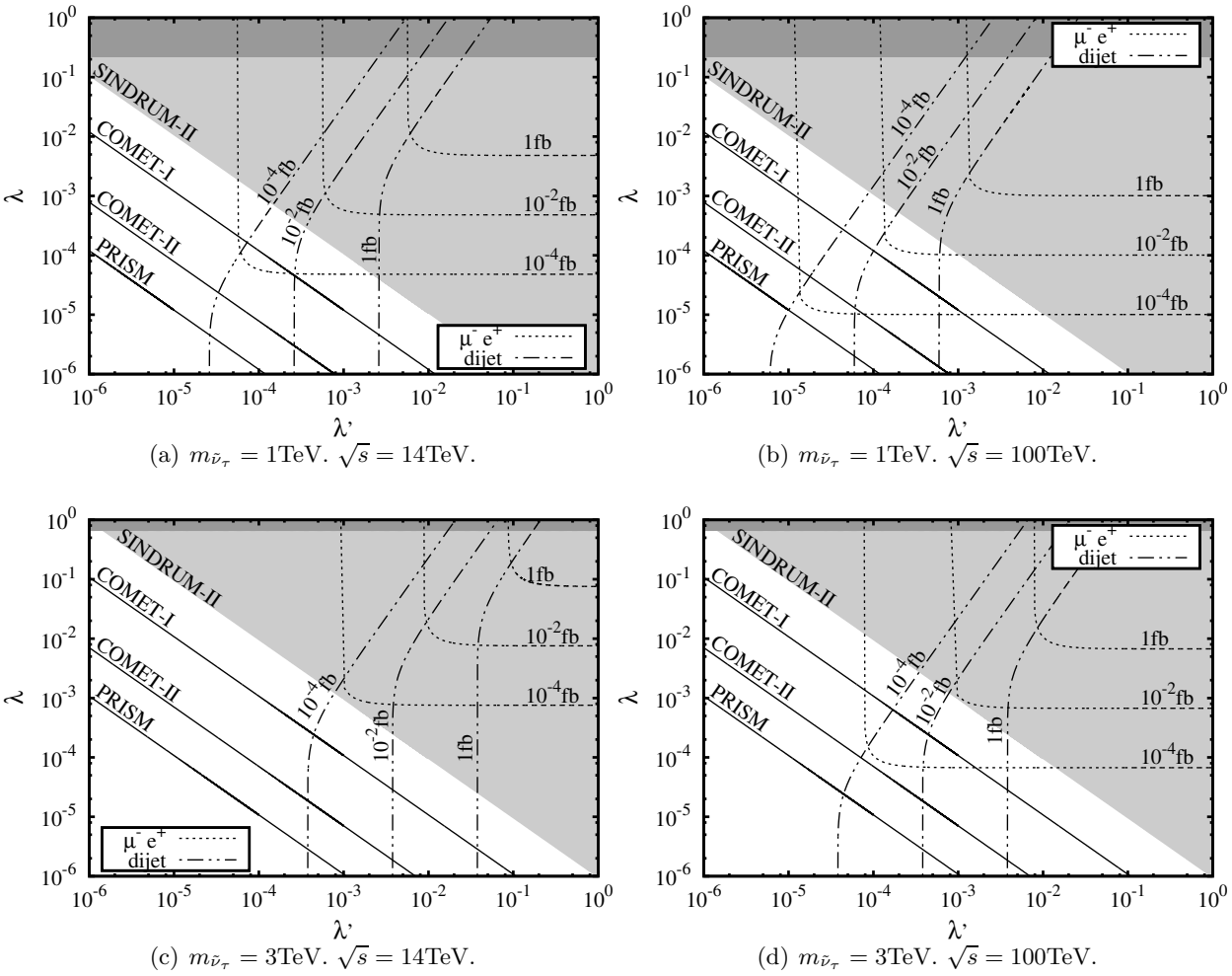

(a) $m_{\tilde{\nu}_\tau} = 1\text{TeV}$. $\sqrt{s} = 14\text{TeV}$. (b) $m_{\tilde{\nu}_\tau} = 1\text{TeV}$. $\sqrt{s} = 100\text{TeV}$.

(c) $m_{\tilde{\nu}_\tau} = 3\text{TeV}$. $\sqrt{s} = 14\text{TeV}$. (d) $m_{\tilde{\nu}_\tau} = 3\text{TeV}$. $\sqrt{s} = 100\text{TeV}$.

Figure 10: Contour plot of $\sigma(pp \to \mu^- e^+)$, $\sigma(pp \to jj)$, and $\text{BR}(\mu^- N \to e^- N)$ in the case-III for (a) $m_{\tilde{\nu}_\tau} = 1\text{TeV}$ and $\sqrt{s} = 14\text{TeV}$ (b) $m_{\tilde{\nu}_\tau} = 1\text{TeV}$ and $\sqrt{s} = 100\text{TeV}$ (c) $m_{\tilde{\nu}_\tau} = 3\text{TeV}$ and $\sqrt{s} = 14\text{TeV}$ (d) $m_{\tilde{\nu}_\tau} = 3\text{TeV}$ and $\sqrt{s} = 100\text{TeV}$. For simplicity, we take universal RPV coupling, $\lambda \equiv \lambda_{312} = \lambda_{321} = -\lambda_{132} = -\lambda_{231}$. Light shaded region is excluded by the μ-e conversion search [4], and dark shaded band is excluded region by the M-$\bar{M}$ conversion search [31].

In such a case, in order to determine λ'_{311} and λ'_{322} separately, we need another measurement, say that of the NSI at next-generation neutrino experiments.

It is said that $\epsilon^S_{\mu e}$ of (10^{-4}) can be searched in near future [34]. However, from the current limit of the branching ratio of $\mu \to e$ conversion it must be less than 10^{-6} which is far below than the expected sensitivity.

We leave the detailed study for future work [33].

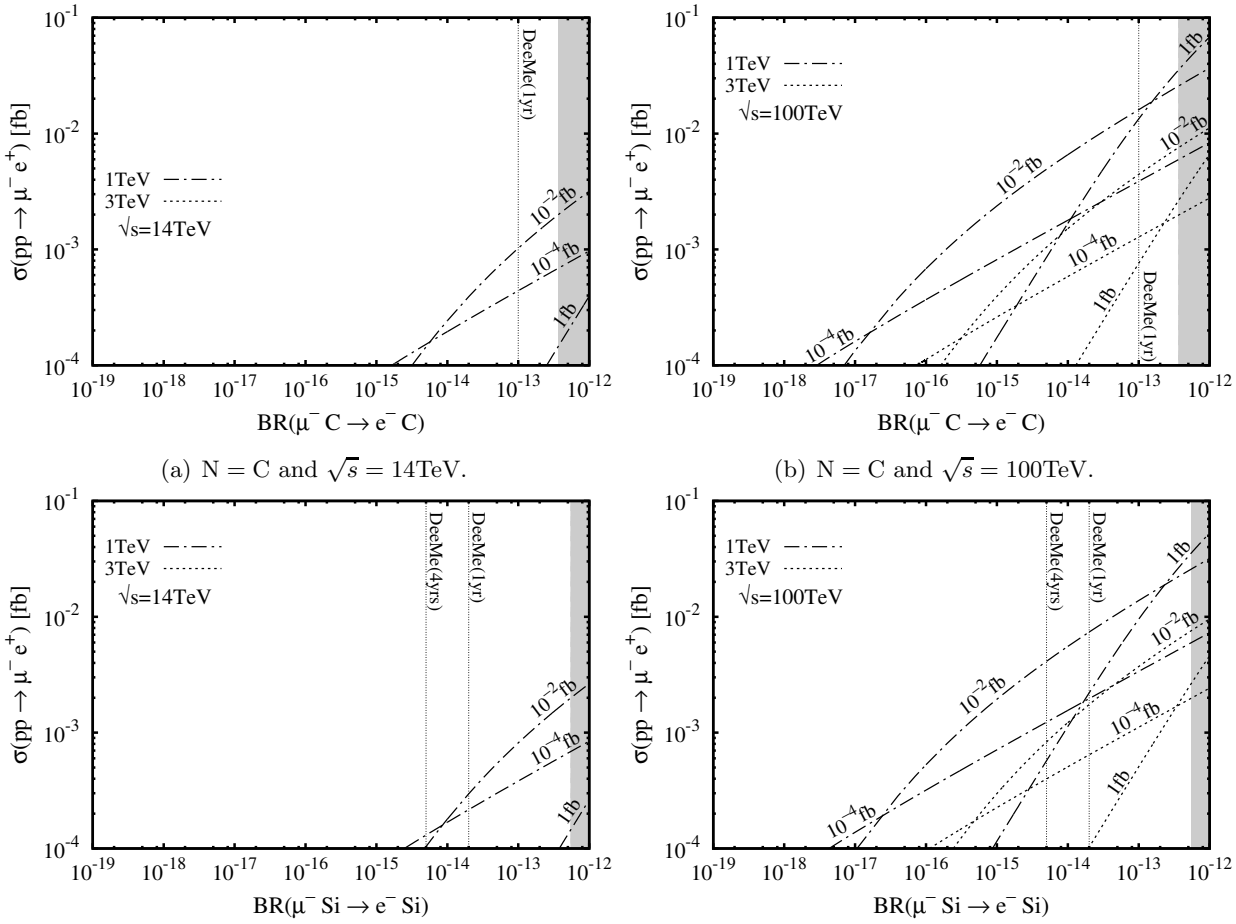

(a) N = C and $\sqrt{s} = 14$TeV.

(b) N = C and $\sqrt{s} = 100$TeV.

(c) N = Si and $\sqrt{s} = 14$TeV.

(d) N = Si and $\sqrt{s} = 100$TeV.

Figure 11: $\sigma(pp \to \mu^- e^+)$ as a function of $\mathrm{BR}(\mu^- N \to e^- N)$ for each $\sigma(pp \to jj)$ in the case-Ⅲ. $\sigma(pp \to jj)$ are attached on each line. Results for $m_{\tilde{\nu}_\tau} = 1$TeV ($m_{\tilde{\nu}_\tau} = 3$TeV) are given by dot-dashed line (dotted line). Shaded region in each panel is the excluded region by the SINDRUM-I I experiment. Left panels show the results for the collision energy $\sqrt{s} = 14$TeV, and right panels show the results for $\sqrt{s} = 100$TeV. We take C [(a) and (b)], and Si [(c) and (d)] for the target nucleus of μ-e conversion process.

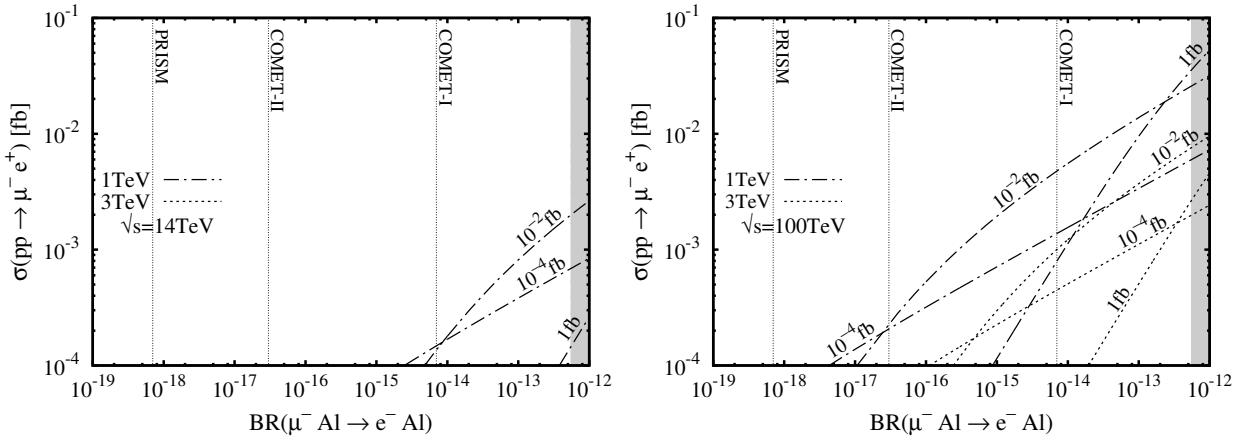

(a) N = Al and $\sqrt{s} = 14$TeV.

(b) N = Al and $\sqrt{s} = 100$TeV.

(c) N = Ti and $\sqrt{s} = 14$TeV.

(d) N = Ti and $\sqrt{s} = 100$TeV.

Figure 12: Same as Fig. 11 except for target nucleus. We take Al [(a) and (b)], and Ti [(c) and (d)] for the target nucleus of μ-e conversion process.

5 Summary and discussion

We have studied a supersymmetric standard model without R parity as a benchmark case that COMET/DeeMe observe $\mu-e$ conversion prior to all the other experiments observing new physics.

In this case with the assumption that only the third generation sleptons contribute to such a process, we need to assume that $\{\lambda'_{311}$ and/or $\lambda'_{322}\} \times \{\lambda_{312}$ and/or $\lambda_{321}\}$ must be sufficiently large. Though other combinations of coupling constants can lead a significant $\mu - e$ conversion process, only those are considered here. This is because in most of scenarios in the supersymmetric theory, the third generation of the scalar lepton has the lightest mass.

With these assumptions, we calculated the effects on future experiments. First we considered the sensitivity of the future $\mu - e$ conversion experiments on the couplings and the masses. To do this we considered the three cases; I) λ'_{311} is dominant, II) λ'_{322} is dominant, III) both are dominant. Since the matrix element of $\bar{q}q$ in nucleus is different for down quark and strange quark, we got a different sensitivity on them.

Then with the sensitivity kept into mind we estimated the reach to the couplings by calculating the cross section of $pp \to \mu^- e^+$ and $pp \to jj$ as a function of the slepton masses and the couplings. To have a signal of $\mu^- e^+$ both the coupling λ' and λ must be large and hence there are lower bounds for them while to observe dijet event via the slepton only the coupling λ' must be large and hence there is a lower bound on it (Figs. 4, 7, and 10). In all cases we have a chance to get confirmation of $\mu - e$ conversion in LHC indirectly. In addition, we put a bound on the couplings by comparing both modes.

On the contrary to the hope on LHC, unfortunately the current bound by $\mu - e$ conversion gives the much smaller Non-Standard Interaction on neutrino physics than the sensitivity in near future experiment. Instead of this fact, with this we can distinguish λ_{312} and λ_{321} and it is worth searching it.

Finally we considered muonium conversion. If λ' is very small we cannot expect a signal from LHC. In this case at least one of λ_{312} and λ_{321} must be very large and if it is lucky, that is both of them are very large we can expect muonium conversion.

There are other opportunities to check the result on $\mu - e$ conversion. For example we can distinguish λ_{312} and λ_{321} in linear collider with polarized beam. We can also expect the signal $pe^- \to p\mu^-$ in LHeC. It is however beyond the scope of this paper to estimate their sensitivities and we leave them in future work [33].

Acknowledgments

This work was supported in part by the Grant-in-Aid for the Ministry of Education, Culture, Sports, Science, and Technology, Government of Japan, No. 24340044 and No. 25105009 (J.S.). and No. 25003345 (M.Y.).

References

[1] Y. Kuno and Y. Okada, Rev. Mod. Phys. **73**, 151 (2001) [hep-ph/9909265].

[2] M. L. Brooks *et al.* [MEGA Collaboration], Phys. Rev. Lett. **83**, 1521 (1999) [hep-ex/9905013].

[3] J. Adam *et al.* [MEG Collaboration], Phys. Rev. Lett. **110**, no. 20, 201801 (2013) [arXiv:1303.0754 [hep-ex]].

[4] W. H. Bertl *et al.* [SINDRUM II Collaboration], Eur. Phys. J. C **47**, 337 (2006).

[5] U. Bellgardt *et al.* [SINDRUM Collaboration], Nucl. Phys. B **299**, 1 (1988).

[6] B. Aubert *et al.* [BaBar Collaboration], Phys. Rev. Lett. **92**, 121801 (2004) [hep-ex/0312027].

[7] K. Abe *et al.* [Belle Collaboration], Phys. Rev. Lett. **92**, 171802 (2004) [hep-ex/0310029].

[8] K. Hayasaka *et al.* [Belle Collaboration], Phys. Lett. B **613**, 20 (2005) [hep-ex/0501068].

[9] Y. Enari *et al.* [Belle Collaboration], Phys. Lett. B **622**, 218 (2005) [hep-ex/0503041].

[10] Y. Fukuda *et al.* [Super-Kamiokande Collaboration], Phys. Rev. Lett. **81**, 1562 (1998) [hep-ex/9807003].

[11] K. Abe *et al.* [T2K Collaboration], Phys. Rev. Lett. **112**, 061802 (2014) [arXiv:1311.4750 [hep-ex]].

[12] R. Aaij *et al.* [LHCb Collaboration], Phys. Lett. B **724**, 36 (2013) [arXiv:1304.4518 [hep-ex]].

[13] Y. G. Cui *et al.* [COMET Collaboration], KEK-2009-10.

[14] Y. Kuno [COMET Collaboration], PTEP **2013** (2013) 022C01.

[15] H. Natori [DeeMe Collaboration], Nucl. Phys. Proc. Suppl. **248-250**, 52 (2014).

[16] J. Hisano, T. Moroi, K. Tobe and M. Yamaguchi, Phys. Rev. D **53**, 2442 (1996) [hep-ph/9510309].

[17] J. Sato and K. Tobe, Phys. Rev. D **63**, 116010 (2001) [hep-ph/0012333].

[18] A. de Gouvea, S. Lola and K. Tobe, Phys. Rev. D **63**, 035004 (2001) [hep-ph/0008085].

[19] S. Weinberg, Phys. Rev. D **26** (1982) 287.

[20] N. Sakai and T. Yanagida, Nucl. Phys. B **197** (1982) 533.

[21] L. J. Hall and M. Suzuki, Nucl. Phys. B **231** (1984) 419.

[22] M. Koike, Y. Kuno, J. Sato and M. Yamanaka, Phys. Rev. Lett. **105**, 121601 (2010) [arXiv:1003.1578 [hep-ph]].

[23] J. E. Kim, P. Ko and D. -G. Lee, Phys. Rev. D **56**, 100 (1997) [hep-ph/9701381].

[24] R. Kitano, M. Koike and Y. Okada, Phys. Rev. D **66** (2002) 096002 [Erratum-ibid. D **76** (2007) 059902] [hep-ph/0203110].

[25] T. S. Kosmas, S. Kovalenko and I. Schmidt, Phys. Lett. B **511** (2001) 203 [hep-ph/0102101].

[26] J. Pumplin, D. R. Stump, J. Huston, H. L. Lai, P. M. Nadolsky and W. K. Tung, JHEP **0207** (2002) 012 [hep-ph/0201195].

[27] A. I. Vaĭnshteĭn, V.I. Zakharov, and M. A. Schifman, JETP vol.**22** (1975) 55 [Pis'ma Zh. Eksp. Teor. Fiz. **22**, No.2 (1975) 123].

[28] T. Ota and J. Sato, Phys. Lett. B **545**, 367 (2002) [hep-ph/0202145].

[29] T. Ota, J. Sato and N. -a. Yamashita, Phys. Rev. D **65**, 093015 (2002) [hep-ph/0112329].

[30] K. Horikawa and K. Sasaki, Phys. Rev. D **53**, 560 (1996) [hep-ph/9504218].

[31] L. Willmann, P. V. Schmidt, H. P. Wirtz, R. Abela, V. Baranov, J. Bagaturia, W. H. Bertl and R. Engfer *et al.*, Phys. Rev. Lett. **82**, 49 (1999) [hep-ex/9807011].

[32] Mu2e Collaboration, *Proposal to search for* $\mu^- + N \to e^- N$ *with a single-event sensitivity below* 10^{-16} *(Mu2e experiment)* (2008). (Available at: http://mu2e-docdb.fnal.gov/cgi-bin/ShowDocument?docid=388).

[33] J. Sato and M. Yamanaka, in preparation.

[34] J. Kopp, M. Lindner, T. Ota and J. Sato, Phys. Rev. D **77**, 013007 (2008) [arXiv:0708.0152 [hep-ph]].